JOURNAL OF GEOPHYSICAL RESEARCH, VOL. 105, NO. B6, PAGES 13,339–13,364, JUNE 10, 2000

Exhumation of ultrahigh-pressure continental crust in east central China: Late Triassic–Early Jurassic tectonic unroofing

Bradley R. Hacker,[1] Lothar Ratschbacher,[2,3] Laura Webb,[4,5] Michael O. McWilliams,[4] Trevor Ireland,[4] Andrew Calvert,[1] Shuwen Dong,[6] Hans-Rudolf Wenk,[7] and Daniel Chateigner[7,8]

Abstract. The largest tract of ultrahigh-pressure rocks, the Dabie–Hong'an area of China, was exhumed from 125 km depth by a combination of normal-sense shear from beneath the hanging wall Sino–Korean craton, southeastward thrusting onto the footwall Yangtze craton, and orogen-parallel eastward extrusion. Prior to exhumation the UHP slab extended into the mantle a downdip distance of 125–200 km at its eastern end, whereas it was subducted perhaps only 20–30 km at its far western end ~200 km away. Structural reconstructions imply that the slab was >10 km thick. U/Pb zircon and $^{40}Ar/^{39}Ar$ geochronology indicate that exhumation up to crustal depths occurred diachronously between 240 and ~225–210 Ma, reflecting a vertical exhumation rate of >2 mm/yr. The upper boundary of the slab is the Huwan shear zone, a normal-sense detachment that reactivated the plate suture. The lower boundary is represented by the Lower Yangtze fold–thrust belt. NW-trending stretching lineations, NE-vergent, WNW–ESE trending <a> folds, dominant top-NW shear, and conjugate, but overall asymmetric, shear band fabrics, document that exhumation was accomplished by updip and orogen-parallel extrusion accompanied by layer-parallel thinning. The orientation and shape of the folds, and a change from SE to SW flow directions, imply that the slab rotated clockwise about a western pivot during exhumation; this rotation was likely caused by the eastward increasing depth of subduction mentioned above, combined with a possible marginal basin and a weak eastern plate boundary. Exhumation of the slab produced considerable shortening in the Lower Yangtze fold–thrust belt, perhaps producing the foreland orocline.

1. Significance of the Study

This paper documents the early deformational and pressure–temperature (P–T) history of the exhumation of the world's largest known tract of ultrahigh-pressure (UHP) rocks, the Dabie–Hong'an area, using new structural, geochronological, and petrological data; the Cretaceous–Recent contribution to the exhumation is detailed by *Ratschbacher et al.* [this issue]. The principal question this paper addresses is as follows: How were these unusual rocks exhumed from depths of 100–150 km? We argue that exhumation was accomplished principally by lithosphere-scale normal shear between 240 and 225–210 Ma.

2. Dabie–Hong'an Area

The Dabie and Hong'an areas comprise part of a 2000 km long orogen formed chiefly in the Triassic by attempted north-directed subduction of the Yangtze craton or a microcontinent before or during collision with the Sino–Korean craton (Figure 1). Investigation of UHP tectonics initially focused on the Dabie Shan because of the wide variety of continental crustal rocks metamorphosed under a complete range of low to ultrahigh P, but work later shifted to include the Hong'an area, where exhumation structures are better preserved. From south to north, the main rock units in Dabie (Figure 2) are the Lower Yangtze fold-thrust belt, blueschist, high-pressure (HP) amphibolite, quartz eclogite, coesite eclogite, Northern Orthogneiss unit, Luzhenguang Group, and Foziling Group. All are intruded by voluminous Cretaceous plutons, and units on the margins of the mountains are overlain by Cretaceous and younger sedimentary and volcanic rocks. The coesite- and diamond-bearing eclogites indicate subduction of continental crust to >120 km [*Liou et al.*, 1996]. The appellations of these units are somewhat misleading, as mafic or ultramafic rocks with the diagnostic HP parageneses constitute only ~5 vol % of an otherwise mostly felsic and chiefly paragneissic sequence.

In the Hong'an area (Figures 1 and 2), blueschist-facies rocks are more widespread, and a distinct eclogite-retrogressed-to-amphibolite unit has been mapped, in addition to quartz eclogite and coesite eclogite. Also, a wider variety of Paleozoic metamorphic rocks crop out in E–W trending fault-bounded units at the northern limit of the range (i.e., the Qinling through Erlangping Groups in the NW corner of Figure 2). Many of these units are best known in the Qinling area (Figure 1) [*Xue et al.*, 1996; *Zhai et al.*, 1998].

3. Ultrahigh-Pressure Petrology

The rock suite in Dabie and Hong'an is chiefly a paragneiss with less granodioritic–tonalitic orthogneiss; the paragneiss

[1]Department of Geology, University of California, Santa Barbara.
[2]Institut für Geologie, Universität Würzburg, Würzburg, Germany.
[3]Now at Institut für Geologie, Technische Universität Bergakademic Freiberg, Freiberg, Germany.
[4]Department of Geological and Environmental Sciences, Stanford University, Stanford, California.
[5]Now at Section des Sciences de la Terre, Université de Geneve.
[6]Chinese Academy of Geological Sciences, Beijing, China.
[7]Department of Geology, University of California, Berkeley.
[8]Now at Laboratoire de Physique de l'Etat Condensé, Universite du Maine, Le Mans, France.

Paper number 2000JB900039.
0148-0227/00/2000JB900039$09.00

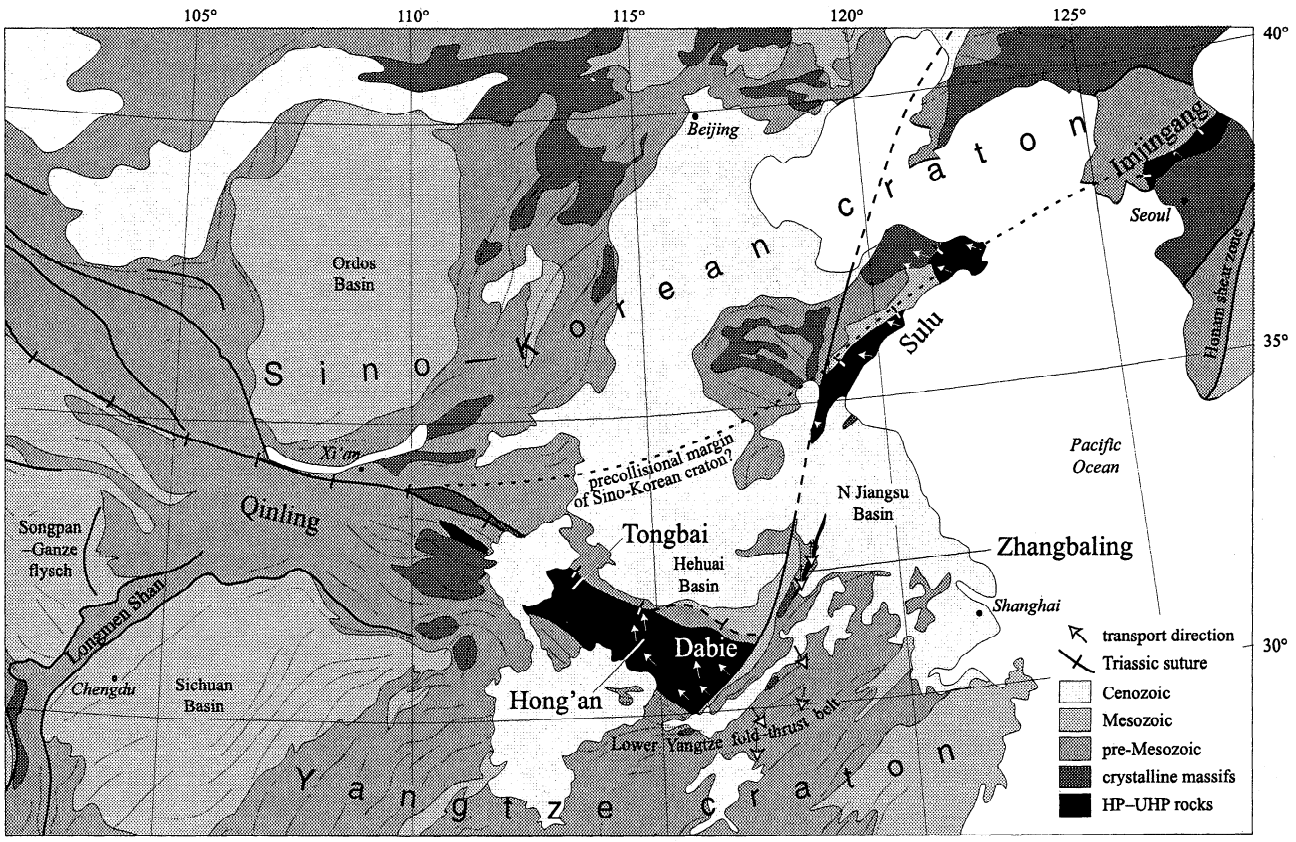

Figure 1. Triassic collisional orogen in central China, after *Ministry of Geology and Mineral Resources* [1991], *Yin and Nie* [1993], and *Ree et al.* [1996].

contains ~5 vol % boudins of eclogite or eclogite retrogressed to garnet amphibolite and epidote–biotite amphibolite. The highest T and P attained in the coesite- and, locally, diamond-bearing [*Xu and Su*, 1997] eclogites were 825°–850°C and 3.3–4.0 GPa [*Carswell et al.*, 1997] (Figure 3). The coesite-free eclogites reached somewhat lower peak conditions of 625°–700°C and 2.2–2.4 GPa in the Dabie Shan [*Okay*, 1993; *Liou et al.*, 1996; *Carswell et al.*, 1997] and have been divided into kyanite-bearing and kyanite-absent eclogites in Hong'an, with estimated physical conditions of 550°–650°C, 1.6–2.5 GPa and 450°–550°C, 0.8–1.2 GPa, respectively [*Eide*, 1993]. The amphibolite unit is a hornblende-rich orthogneiss; peak P and T estimated from one locality are >1.0 GPa and ≤650°C [*Liu and Liou*, 1995]. Blueschists reached conditions of only 400–800 MPa at 350°–450°C [*Eide*, 1993; *Eide and Liou*, 2000]. While most of the UHP thermobarometry derives from mafic blocks within the felsic paragneiss, the paragneiss also locally contains unambiguous indications of metamorphism at similar P and T, such that the eclogites clearly were metamorphosed in situ [*Liou et al.*, 1996]; the same may not hold true for ultramafic blocks, some of which record recrystallization pressures >4 GPa [*Okay*, 1994; *Hacker et al.*, 1997; *Liou and Zhang*, 1998]. The coesite-eclogite and quartz-eclogite units experienced strong recrystallization at amphibolite-facies conditions, typified by the stability of hornblende + plagioclase + sphene in mafic rocks and muscovite + biotite + epidote + plagioclase + orthoclase + quartz ± garnet in the quartzofeldspathic gneisses; likewise, the amphibolite unit underwent an albite-epidote-amphibolite facies retrogression.

We discovered one new eclogite in the NE part of Hong'an (locality D228, Figure 2) that has important structural implications detailed in section 4. Fe–Mg exchange between garnet and included omphacite crystals suggests a peak T of 725°C, using either the *Ellis and Green* [1979] or *Ravna* [1998] formulations, while rims of adjacent garnet and omphacite matrix grains indicate 625°C. Pressures, calculated for Mg-tschermak exchange among muscovite, garnet, and clinopyroxene using Thermocalc [*Holland and Powell*, 1998], are 1.5 GPa for both the inclusion suite and the rim compositions, just greater than minimum P calculated for the jadeite component of omphacite (1.4 and 1.5 GPa).

4. Structural Geology

4.1. Overview

The HP to UHP rocks of the Dabie Shan are essentially a structural homocline with SE to SW dipping foliation, SE plunging lineation, and overall top-to-NW flow that includes significant coaxial stretching (Figure 4). This same general structure is also present in Hong'an, with two important differences. Most significantly, in northern Hong'an the south oriented structures roll over through horizontal into N(W) dipping foliations, N(W) plunging lineations, and N(W) directed sense of shear. The distribution of metamorphic rocks in Hong'an also reflects this antiformal structure. The pseudostratigraphy of the Hong'an area also defines a series of kilometer-scale NW trending synforms and antiforms that are overturned to the north in central Hong'an, and are upright to south facing in southern Hong'an. The coesite-bearing eclogite unit forms the core of the northernmost antiform; the lowest-P rocks, blueschist, are present

only on the south limb of this orogen-scale fold. The presence of quartz eclogites in the Sujiahe Group [*Liu et al.*, 1996] and in NE Hong'an (our locality D228, Figure 2) is key to recognizing this structure because it affirms that quartz eclogites crop out north and south of the coesite eclogites. The westward decrease in peak metamorphic pressures reveals that the antiform plunges west; the east edge of the antiform is truncated by the Tan–Lu fault.

The structures visible in Hong'an are not seen in Dabie because of strong Cretaceous magmatism and extension [*Ratschbacher et al.*, this issue]. Briefly, the Dabie Shan underwent NW directed extension at ~140–120 Ma approximately coeval with the intrusion of gabbroic through syenitic plutons. The largest structure associated with this extension is the Xiaotian–Mozitang fault, a north dipping sinistral transtensional fault (Figure 2). The Cretaceous plutonism was so extensive that it formed a large Northern Orthogneiss complex that obliterated nearly all the UHP rocks in the northern half of the Dabie Shan [*Ratschbacher et al.*, this issue; *Tsai and Liou*, 2000]. To aid in understanding the Triassic–Jurassic evolution of the study area, Figures 10 and 12 use the pre-Cretaceous palinspastic restoration of *Hacker et al.* [1998], which is based on ~100% (70 km) extension along a 325° trend.

Our structural data supporting this overview are detailed in the remainder of this section and are summarized in Figures 4–9 and Table 1. In four field seasons we characterized on a regional scale the internal deformation and contacts of each of the main rock units by studying the relative amount of deformation, the sense of displacement or shear, and the P and T of deformation. The latter were judged by assessing which minerals or melts formed before, during, or after structures observed at the outcrop to electron microscope scale. The amount of deformation was judged from the shape of deformed objects such as xenoliths or crystals, the discrete displacement or distributed shear of markers such as dikes, the thickness and spacing of deformed zones, and the degree of grain-size reduction. Sense of shear was established in the field and in thin section by criteria such as offset markers, σ clasts, δ clasts, shear bands, asymmetric boudinage, schistosité-cisaillement (S-C) fabrics, and lattice preferred orientation (texture) measurements of calcite and quartz. In particular, we used quartz textures extensively for deformation path and flow temperature interpretations; these interpretations are based on comparisons with textures from deformation zones worldwide where the path and the temperature have been established by independent criteria, and with textures derived from polycrystal

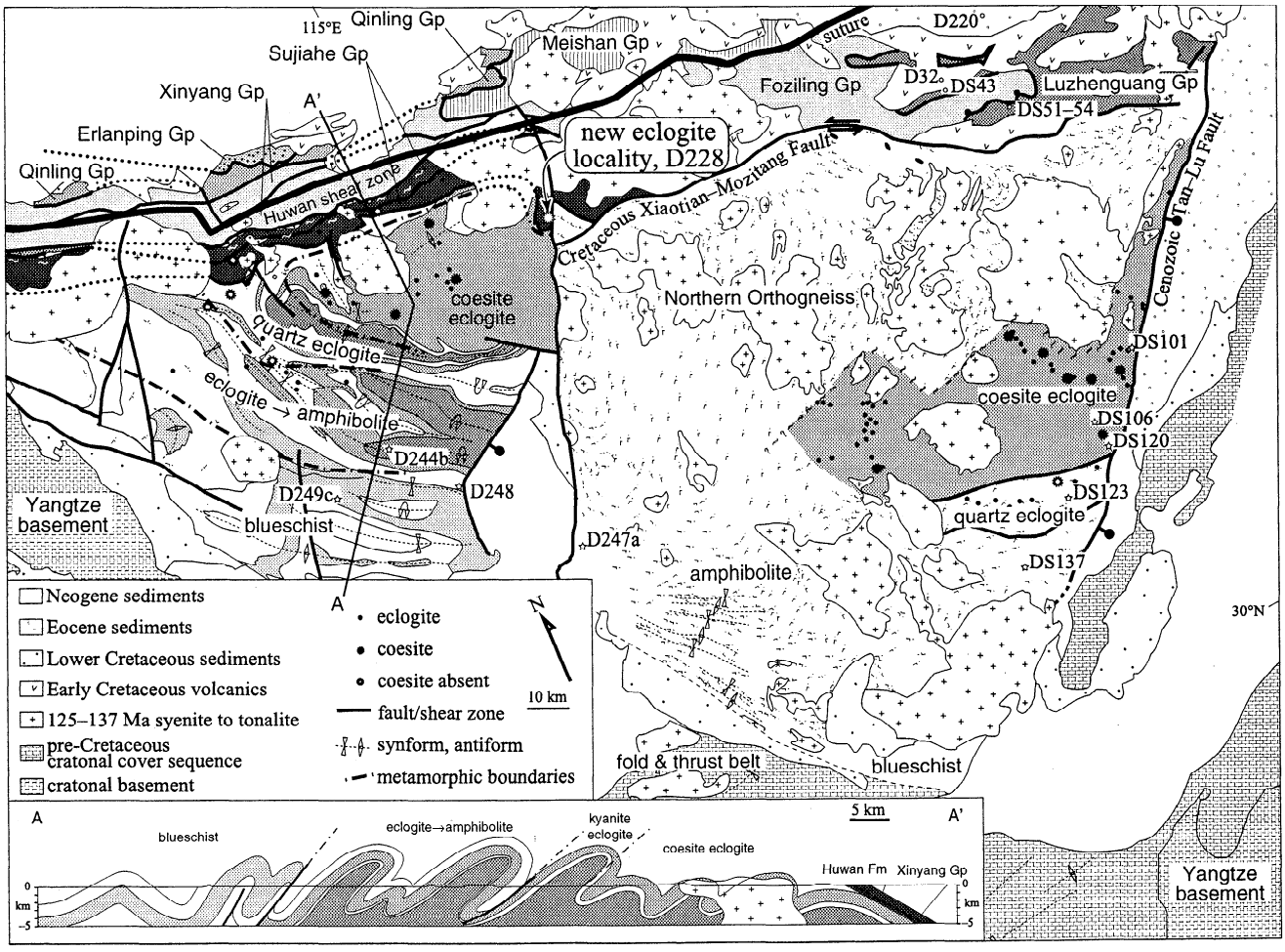

Figure 2. Map of the Dabie Shan and Hong'an areas, drawn from our fieldwork in 1991–1995, *Regional Geological Survey of Anhui* [1987], *Regional Geological Survey of Henan* [1989], *Regional Geological Survey of Hubei* [1990], and *Okay et al.* [1993]. Coesite/quartz and eclogite locations are from our work plus that of *Eide* [1993], *Zhou et al.* [1993], *Cui and Wang* [1995], *Liou et al.* [1996], and *Liu et al.* [1996]. Locations of hornblende and K-feldspar $^{40}Ar/^{39}Ar$ samples are shown with D prefix. Diffuse shear zone between Northern Orthogneiss and coesite eclogite units is shown schematically; see *Ratschbacher et al.* [this issue] for detail. Gray shading emphasizes different units.

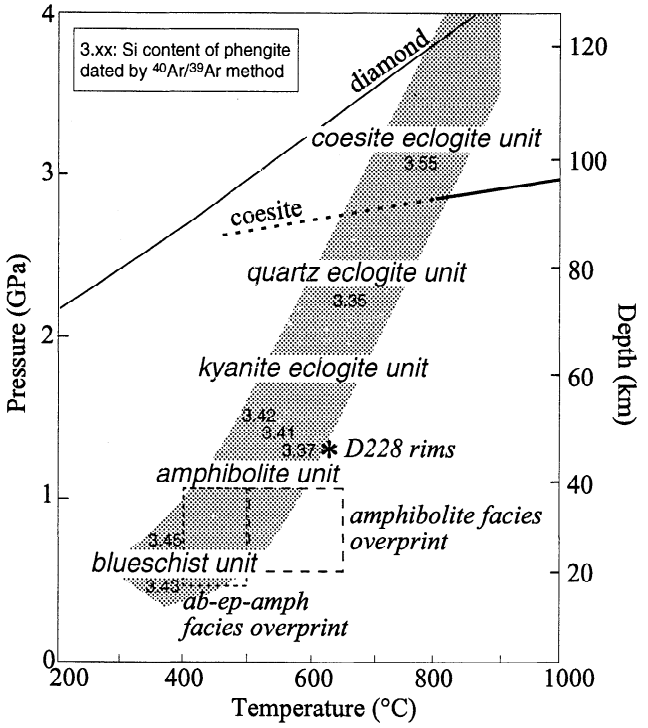

Figure 3. Peak P and T for Dabie–Hong'an rock units [*Eide*, 1993; *Okay*, 1993; *Liu and Liou*, 1995; *Liou et al.*, 1996; *Carswell et al.*, 1997]; P gaps within the sequence are not shown. Numbers, 3.30–3.55, show number of Si atoms per formula unit of phengite within paragneisses dated in this study (compare Figure 11b). "Amphibolite-facies overprint" refers to retrogression of eclogite units; "ab-ep-amph" refers to late albite-epidote-amphibolite-facies overprint of amphibolite unit. Depths are computed assuming 40 km crust of 2.7 g/cm^3 overlying mantle of 3.3 g/cm^3.

plasticity models and experimental data. To understand the kinematics of fault arrays, we applied "stress" inversion techniques to mesoscopic fault slip data. We refer the reader to *Passchier and Trouw* [1996], *Angelier* [1994], and *Twiss and Unruh* [1998] for recent, comprehensive summaries and critical discussions of these methods.

4.2. Central Eastern Dabie

Along the northern margin of the coesite-eclogite unit in Dabie, the foliation dips 25°–45° toward 120°–160°; lineations plunge 10°–50° down the dip of the foliation (Figures 4 and 5). Deformation was penetrative, regionally homogeneous, and high strain. Foliations are locally (e.g., locations D63–D69 and D93–D96) bent around Cretaceous plutons. Outcrop-scale isoclinal, recumbent folds with axes subparallel to the stretching direction (<a> folds, *Malavieille* [1987]) are mostly north vergent. Shear bands, σ clasts, S–C fabrics, and quartz *c* and *a* axis textures indicate a top-NW sense of shear at all localities where sense of shear could be determined. When the rocks passed through the ductile-brittle transition, coaxial stretching and top-SE backflow occurred locally (e.g., D73–D74, D86). The kinematic history began in the garnet stability field and extended down temperature to the youngest, brittle–ductile, chlorite-bearing veins. Spectacular outcrop-scale, asymmetric boudins with ≤20 cm thick, partly mylonitized, quartz–biotite–K-feldspar ± hornblende-filled necks developed during late-stage amphibolite- to greenschist-facies conditions. The well-developed foliation and, in particular, lineation, qualitatively indicate plane to constrictional strain. In zones of lower amphibolite to upper greenschist facies retrogression, strain is heterogeneous, with both L and S fabrics, the latter are exemplified by local boudinage in *YZ* sections (*X*≥*Y*≥*Z*, principal strain axes).

Quartz textures also record the top-NW shear during high-T flow. Prismatic *a* slip, indicated by a *c* maximum parallel to *Y*, reported from amphibolite-facies rocks worldwide [e.g, *Schmid and Casey*, 1986], was dominant in quartz of the coesite-eclogite unit. Some rocks have evidence of *c* and *a* prism glide (Figure 5): DS102 and DS158, both typical plagioclase + biotite + garnet ± hornblende UHP paragneisses, the latter from an eclogite–paragneiss intercalation, show a *c* axis maximum parallel to the stretching lineation and a consistent weak *a* axis girdle normal to the *c* maximum, in addition to the texture typical for prismatic *a* slip (*c* axes parallel to *Y* and several *a* maxima distributed in a great circle around *Y*). Prismatic *c* slip occurred exclusively in the UHP rocks of central Dabie and was not observed outside the coesite-eclogite unit. *Mainprice et al.* [1986] and *Blumenfeld et al.* [1986] inferred that high-T (>650°C) and hydrous conditions are required for prism *c* slip, on the basis of natural observation and experiments [*Linker et al.*, 1984].

Table 1. Location of Stations and Parameters of the Deviatoric Stress Tensor

Site	Lithology	N Latitude	E Longitude	Method	Measurements	σ_1	σ_2	σ_3	F	R
D35 b–d	marble, basement*	31°18.01	116°30.25	P-B-T	22/22	183 44	033 41	289 15		
D35 b				NDA	16/16	252 27	082 62	344 04	18	0.7
D36	orthogneiss*	31°16.7	116°48.7	P-B-T	7/7	064 29	280 55	169 14		
D73–74	paragneiess and orthogneiss*	30°40	116°27	NDA	18/18	295 87	026 01	116 03	09	0.5
D86–87-1	orthogneiss	30°44.27	116°01.13	P-B-T	17/17	004 24	154 62	273 14		
D86–87-2				P-B-T	11/13	313 32	071 37	192 35		
D236–237	paragneiss	31°30	114°40	P-B-T	22/22	120 75	275 15	005 05		
D255old	paragneiss*	31°28.24	114°07.63	NDA	25/26	231 66	121 09	027 22	26	0.4
D255you				NDA	19/20	107 62	234 17	331 21	22	0.8
D283-1	limestone	30°06.91	116°02.99	P-B-T	7/7	004 15	183 75	296 06		
D284-1	limestone	30°11.71	116°06.39	P-B-T	22/22	348 21	211 63	086 16		
D285old	limestone	30°15.66	115°23.34	NDA	11/11	354 04	201 85	084 02	19	0.5
D287old	limestone	30°37.36	117°51.72	P-B-T	10/10	311 07	088 80	243 09		

Method: P-B-T, pressure–tension axes [*Turner*, 1953]; NDA, numerical dynamic analysis [*Spang*, 1972]. Measurements: number of data used and total number of data. Here σ_1, σ_2, and σ_3,are azimuth and plunge of major, intermediate, and minor stress axes. *F*, fluctuation, is the average angle between the measured slip direction and the orientation of the calculated shear stress. *R*, stress ratio, is $(\sigma_2-\sigma_3)/(\sigma_1-\sigma_3)$, where 1 is uniaxial extension, and 0 is uniaxial shortening.

* Corresponding age(s) given in Table 3.

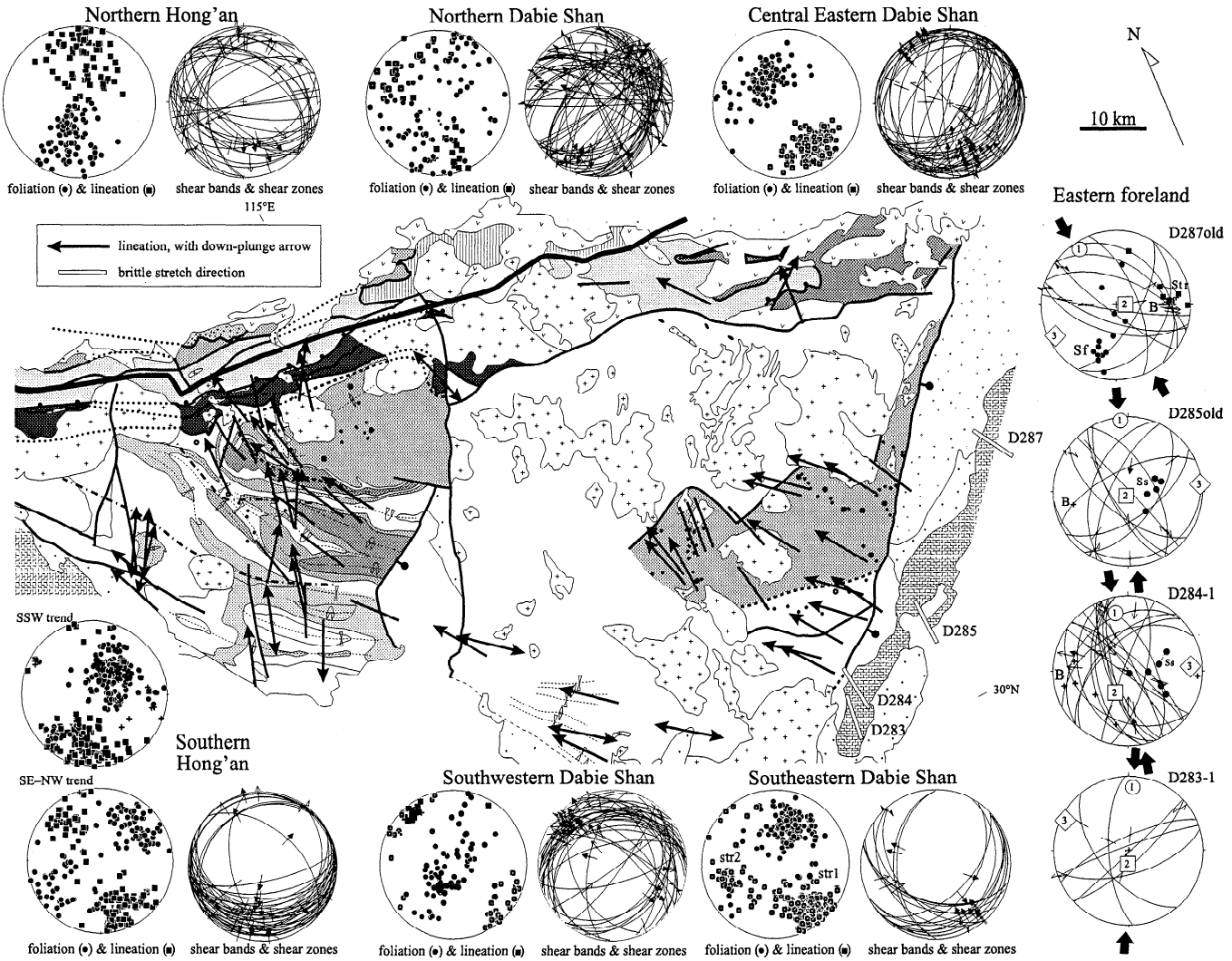

Figure 4. Structural overview of the Dabie–Hong'an area. Areas disturbed by Cretaceous plutons are not included in the synoptic stereonets. In these and subsequent stereonets showing brittle faults, type of arrowhead shows confidence of sense-of-slip determination: solid arrow, absolutely certain; open arrow, certain; partial arrow; probable; no arrow; inferred.

4.3. Southern Dabie

Foliation in this domain has typical dips of 30°–70° toward 180°–225°; considerable bending of the foliation resulted from folds that parallel the stretching lineation (Figures 4 and 6). The southern part of the coesite-eclogite unit contains a single lineation that plunges 0°–30° toward 130°–150°, but the quartz-eclogite and amphibolite units contain two lineations. The first, defined by competent phases such as garnet and hornblende, with strain shadows locally filled by oriented phengite, is often barely visible, and plunges 0°–45° toward 125°–160°; anastomosing shear zones around eclogite boudins show locally coaxial stretching along this lineation, but an overall top-NW sense of shear is indicated by the asymmetry of the anastomosing pattern. The second lineation postdates a relatively static amphibolite-facies recrystallization, and developed during cooling through lower amphibolite to greenschist-facies conditions, marked by the growth of albite, muscovite, epidote, and chlorite. The second lineation is defined by stretched quartz grains, visible in quartz, quartz + chlorite, and quartz + K-feldspar + magnetite + tourmaline veins, and plunges 15°–40° toward 240°–260°. The sense of shear is top-NE, imparting an apparent sinistral sense of motion on the foliation. Although the lineations cluster around two maxima, they form a continuum from early SE plunging through late SW plunging directions. As in central Dabie, folds with axes parallel to the first lineation and NE vergence are widespread.

The SW margin of Dabie contains amphibolite-facies biotite-plagioclase-quartz ± hornblende gneisses retrogressed to greenschist facies. The foliation dips are dispersed at all angles (though mostly steep) in a girdle from 040°–220° by lineation-parallel folds (Figures 4 and 6). Stretching lineations developed in the bulk rock at amphibolite-facies conditions and in biotite + epidote + quartz + chlorite veins, plunge 0°–20° toward 130°–150° and 310°–330°. Where well developed, the sense of shear is also top-NW. L tectonites are particularly common in the southwest.

Quartz textures show that prismatic *a* slip was confined to the coesite eclogite unit (e.g., D75), whereas basal *a* slip was

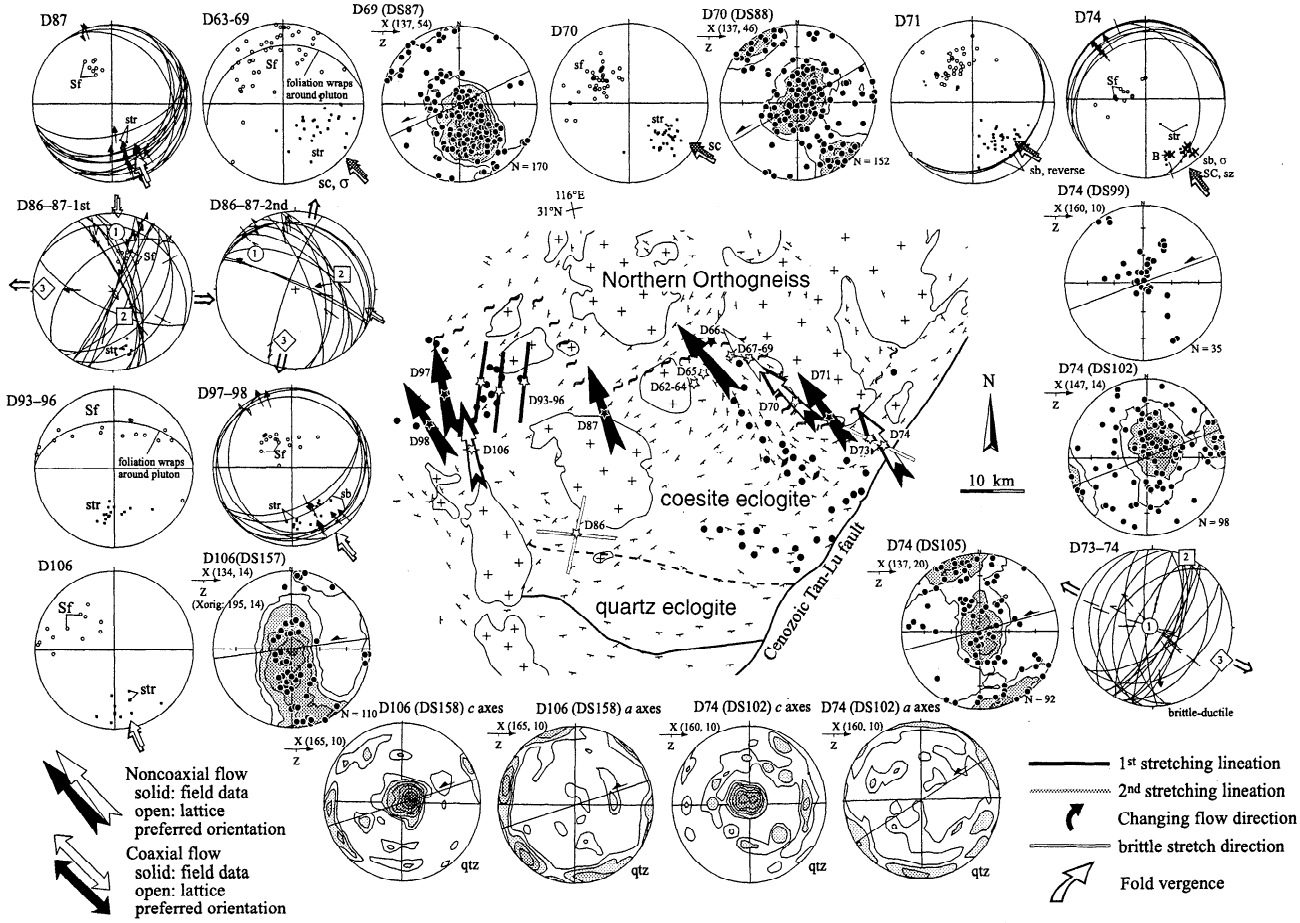

Figure 5. Structural data from northern margin of the coesite-eclogite unit in Dabie. Sf, foliation; str, stretching lineation; *B*, fold axis; sb, shear band; SC, S-C fabric; sz, shear zone; σ, sigma clast; δ, delta clast; *X*, *Z*, principal axes of finite strain; ab, asymmetric boudinage; 1 and 2, first and second deformation fabric elements; cc, calcite; and qtz, quartz. All are lower hemisphere, equal-area diagrams. Lattice preferred orientations were derived from x-ray goniometry (shading alone) and U-stage measurements (dots and shading). Solid boundaries are well located; dashed boundaries are poorly located.

predominant in the amphibolite unit (e.g., D113). These quartz textures are associated with the first stretching lineation, even in outcrops where the first lineation is nearly erased by the second lineation (e.g., DS126). Both the planar shear criteria (shear zones, shear bands, and S-C fabrics) and the quartz textures demonstrate a more heterogeneous, and distinctly more coaxial, deformation in southern Dabie than in the UHP rocks of central eastern Dabie. Overall, shear was top-NW; however, conjugate shear bands, shear zones, and orthorhombic quartz textures are common. Locally, top-SE backflow dominated (e.g., D114).

4.4. Northern Dabie

The Foziling and Luzhenguang "Groups" crop out north of the Cretaceous sinistral transtensive Xiaotian–Mozitang fault as the leading north edge of the Yangtze craton [see *Hacker et al.*, 1995, 1998; *Ratschbacher et al.*, this issue]. Restoring the Cretaceous extension and Triassic normal shear along the eastern prolongation of the Huwan shear zone (section 4.6) places these units at a middle to upper crustal level. At the few localities where we examined these units, the foliation and stretching lineation are highly variable, probably because of multiple, particularly Cretaceous, refolding [*Ratschbacher et al.*, this issue]. The foliation generally dips NE and SW (Figures 4 and 7), the stretching lineation plunges NE to NW, but probably mostly north before refolding. Sinistral shear zones, containing low-T quartz mylonites with <a> folds and breccia formed under high fluid pressure, were encountered at two localities. The Foziling overlies the Luzhenguang along a refolded low-angle shear zone that shows movement of the hanging wall down to the NW–NE. Deformation started at high T in the Luzhenguang with dominant prismatic *a* slip in quartz (samples DS53 and DS44) and continued into low-T plasticity with similar but complex kinematics (calcite texture of sample DS44 and faulting at stations D35–D36). The overall pattern is similar to the northern margin of the Hong'an area (section 4.6), i.e., top-north normal shear, but deformation was more distributed and heterogeneous.

4.5. Southern Hong'an

Exposures in Hong'an (Figures 8 and 9) define the orogen-scale antiform mentioned in section 4.1. The southern limb of the antiform dips southward at ~30°, whereas the northern limb dips more steeply northward at ~70° (Figure 2).

Outcrops along the better-exposed southern side of Dawu dome provide examples of the deformation style exhibited from the thin-

section to the orogen scale, i.e., boudinage resulting from high-strain extension along the mineral lineation. The dome has a core of unretrogressed, two-mica orthogneiss rimmed by heterogeneously and strongly deformed metasedimentary rocks. We interpret the dome as the result of vertical flattening and megaboudinage produced by subhorizontal, N–S extension during dominantly coaxial flow. The boudinage is particularly well illustrated in the metasedimentary rocks by conjugate shear zones with interplanar angles as small as 20° (D253–D255), indicating extreme flattening. The low temperature of the deformation and the young mineral cooling ages [~200 Ma, *Webb et al.*, 1999] indicate that this doming developed late in the exhumation history.

The blueschist rocks of Mulan Shan (stations D249–D252) developed out of acid to intermediate volcanic rocks widespread on the Yangtze craton [*Ernst et al.*, 1991]. A first deformation (D1) produced a foliation that is folded into SW and NE dips around folds whose axes are subparallel to a generally NNW trending stretching lineation; the lineation in general has a more northerly trend than the fold axes. The folds are distinctly NE vergent and are associated with a second foliation and stretching lineation, both inclined to the SW. The sense of shear changed from top-NW to top-NE during this progressive deformation (D1 to D2), which was all within the glaucophane stability field. The quartz *c* axis texture of D249b reflects basal+prismatic *a* slip during both D1 and D2; the extension direction defined by the *c*-axis-free area and the normal to the *YZ* girdle is intermediate between the first and second lineations measured on the sample.

Stations D239–D245 investigate one of the overturned, isoclinal, NW plunging domes of central Hong'an (Figure 9). The western side of the plunging dome is a retrogressed L tectonite orthogneiss with spectacular, late-stage plagioclase growth. The low-T quartz *c* axis texture (D239a) suggests top-NNE flow late in the deformation history. A strongly retrogressed eclogite–paragneiss association along the south side of the dome (D240–D241) includes a low-T quartz ribbon mylonite. During cooling within the biotite and chlorite stability fields, flow changed from early top-WNW to late top-north. The early WNW plunging lineation parallels the lineation in the relict eclogite. Early flow

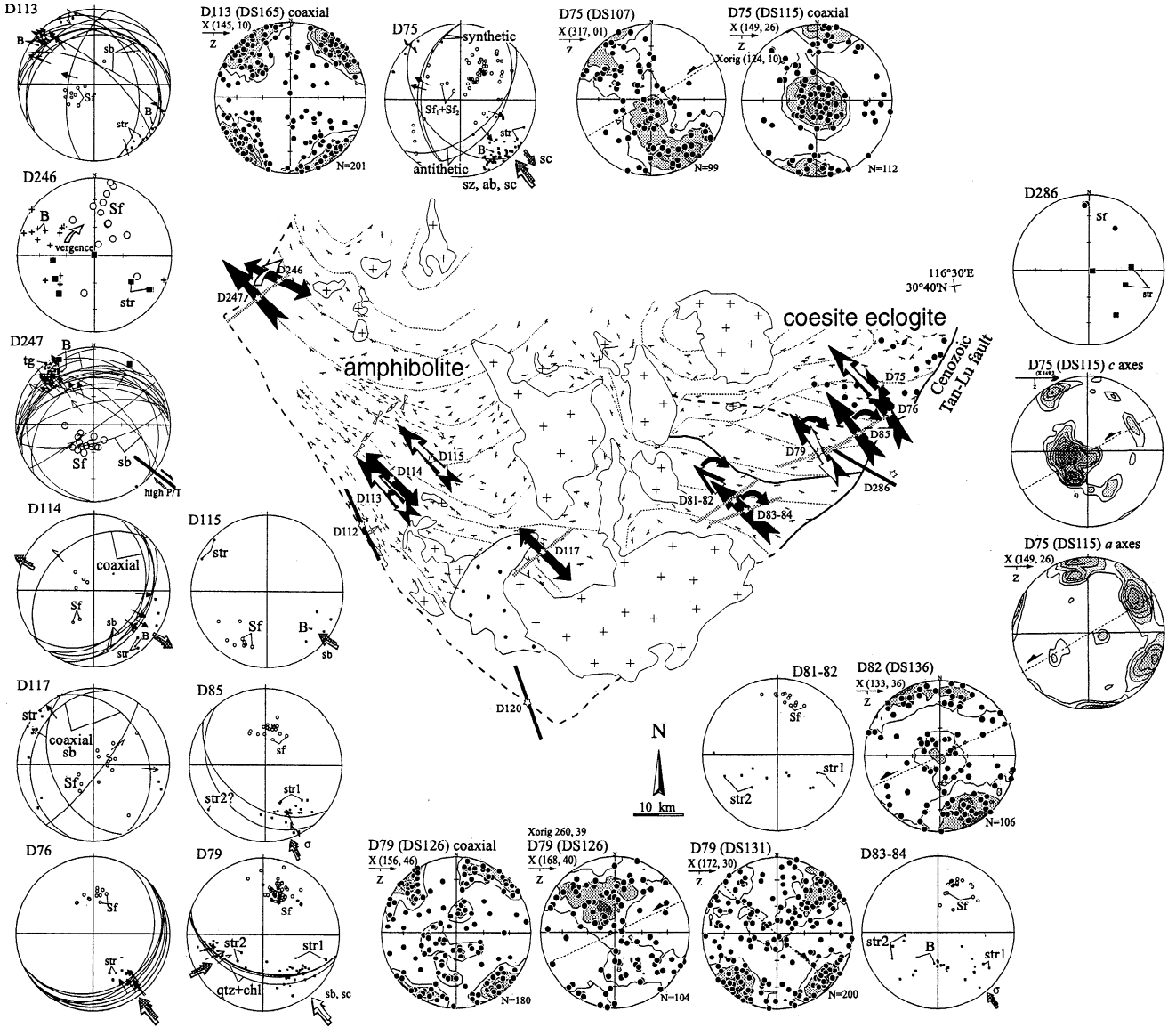

Figure 6. Structural data from southern Dabie. See caption of Figure 5.

was probably close to simple shear (single-girdle quartz texture of D240b [c.f. *Schmid and Casey,* 1986]), and late brittle–ductile shear zones (D241) testify to coaxial stretching within the foliation and parallel to the stretching lineation. The northern, inverted limb (D244–D245) shows similar structural geometry and kinematics. Mica ages of ~235 Ma place this deformation early in the exhumation history.

The NW trending southern boundary of the eclogite → amphibolite unit in south central Hong'an is a zone of enhanced retrogression (albite + epidote + phengite + quartz, and extensive quartz veining) associated with top-north to top-NE vergent folding and shear, i.e., apparent thrusting. It has been mapped discontinuously by *Webb et al.* [2000] from central Hong'an to eastern Tongbai. At nearly all stations along this zone (D242–D243, D244–D255, and D248), early top-(W)NW flow along SW dipping foliations was subparallel to spectacular <a> folds, indicating apparent dextral transpression. During cooling the mineral lineation progressively rotated from a north into a local NE trend, normal to the fold axes and imposing apparent sinistral transpression. Local second foliations dip always slightly more westward than the first foliation, and associated folds have a distinct north to NE vergence.

Stations D233–D238 characterize deformation in the coesite- and kyanite-eclogite units and reveal structural geometries and kinematics identical to the UHP rocks of Dabie. Deformation proceeded from amphibolite facies (in retrogressed eclogite) to upper crustal conditions (shear zones along late quartz + biotite + K-feldspar veins) with the same top-north kinematics. Stations D234–D237 present an analysis of the northernmost, large-scale dome, which constitutes the lowest structural level of the Hong'an antiform, where the predominantly south inclined structures south of the dome roll over into north inclined structures to the north. Structural data from UHP paragneiss and orthogneiss and mica schist document folding of the stretching lineations across the NW trending dome axis and the large-scale boudinage typical of the UHP rocks.

4.6. Northern Hong'an

Along the northern limb of the Hong'an antiform, foliation dips north, and lineation plunges north to NE (Figures 4, 7 and 9). The northern edge of the Hong'an block is marked by the Huwan shear zone, a ~5 km thick, amphibolite–greenschist facies, normal-sense shear zone separating eclogite-facies rocks in the footwall from greenschist-facies rocks in the hanging wall [*Rowley and Xue,* 1996; *Webb et al.,* 2000]. The shear zone contains strongly retrogressed eclogite boudins (e.g., station D231, the low-T quartz textures are from a sheared quartz vein in an eclogite-bearing micaschist). The Huwan shear zone can be followed, with interruptions by Cretaceous plutons, into northern Dabie (Figures 4 and 7), where it is truncated by a large Cretaceous pluton and a strand of the Cretaceous Xiaotian–Mozitang fault zone.

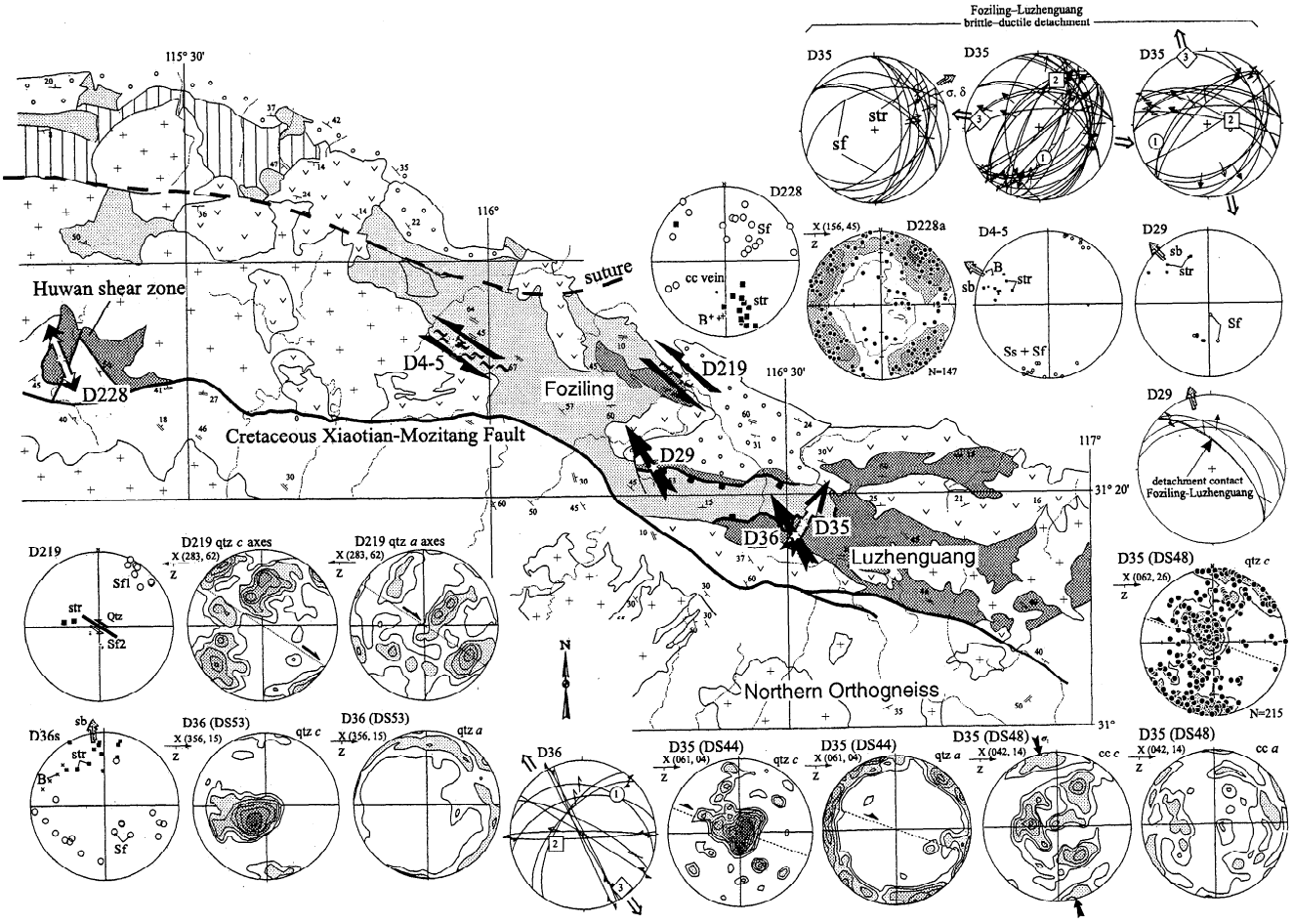

Figure 7. Structural data from northern Dabie. See caption of Figure 5.

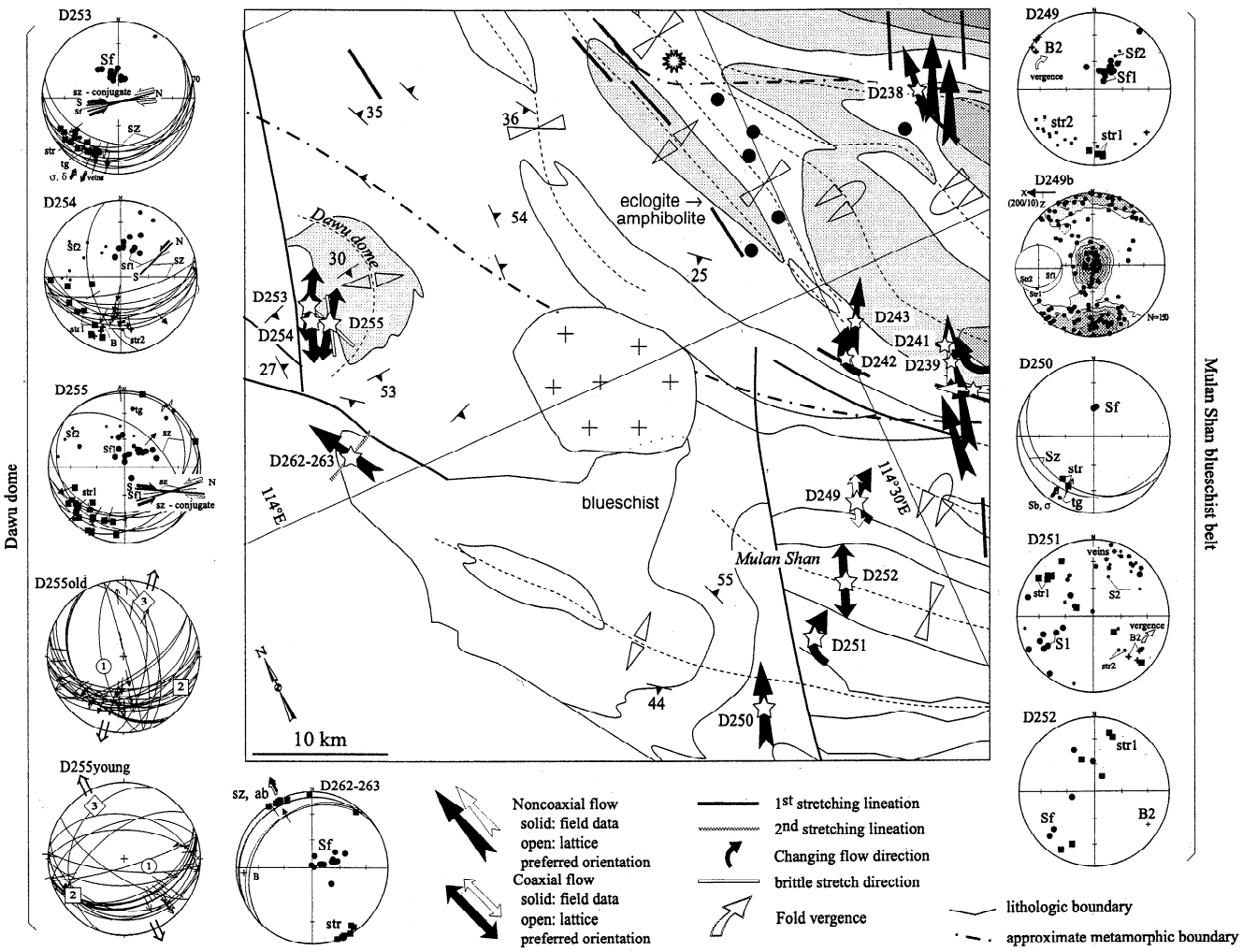

Figure 8. Structural data from southern Hong'an. See caption of Figure 5. Unlabeled data are from *Webb et al.* [2000].

Ratschbacher et al. [this issue] speculate that the Xiaotian–Mozitang fault zone exploited the crustal heterogeneity imposed by the Huwan shear zone to localize large-scale Cretaceous crustal extension.

4.7. Dabie Foreland: The Lower Yangtze Fold–Thrust Belt

We collected a large data set on Triassic–Jurassic faulting and folding in the Lower Yangtze fold–thrust belt, which constitutes the foreland of the Dabie Shan. A few of these data and their interpretations from stations close to Dabie are plotted in Figure 4 and summarized in Table 1; see *Schmid et al.* [2000] for a complete evaluation. The mesoscale faults demonstrate overall N(W)–S(E) subhorizontal contraction. Extension directions are also subhorizontal and indicate along-strike lengthening of the fold belt. Contraction directions in the foreland are thus similar to the stretching lineations in Dabie–Hong'an. We interpret the N(W)–S(E) contraction to be Middle to Late Triassic [*Schmid et al.*, 2000].

4.8. Folds of Hong'an–Dabie

The major train of NW trending, NE overturned folds mapped by Chinese geologists [see references in Figure 2] constitute the most striking feature of Hong'an; such folds are also characteristic of Dabie but are less well mapped. Our deformation analysis shows that folding on all scales most likely occurred during progressive top-NW shearing and the fold axes developed subparallel to the shear direction.

Lineation-parallel folds may either be sheath folds [*Cobbold and Quinquis*, 1980] or straight, so-called <a> folds oblique or parallel to the regional stretching direction [*Mattauer*, 1975; *Malavieille*, 1987]. Mechanisms suggested for the formation of <a> folds are as follows: (1) local or regional constrictional strain [*Mattauer*, 1975; *Ratschbacher and Oertel*, 1987], (2) rotation of folds from an initial high-angle to final low-angle divergence from the extension direction [e.g., *Sanderson*, 1973], and (3) shearing of initially dipping competent layers, i.e., the existence of an angle between the layers and the intermediate shortening axis (*Y*) of finite strain [e.g., *Watkinson*, 1975]. *Froitzheim* [1992] extended the latter case to show that folds with variable but generally stretching-parallel axes can form during extension with contemporaneous development of normal faults and extensional shear zones.

Reorientation of formerly stretching-perpendicular folds seems unlikely in Hong'an–Dabie, because a range of axis orientations has not been observed. Local constriction probably explains some stretching-parallel folds, but our qualitative evaluations indicate

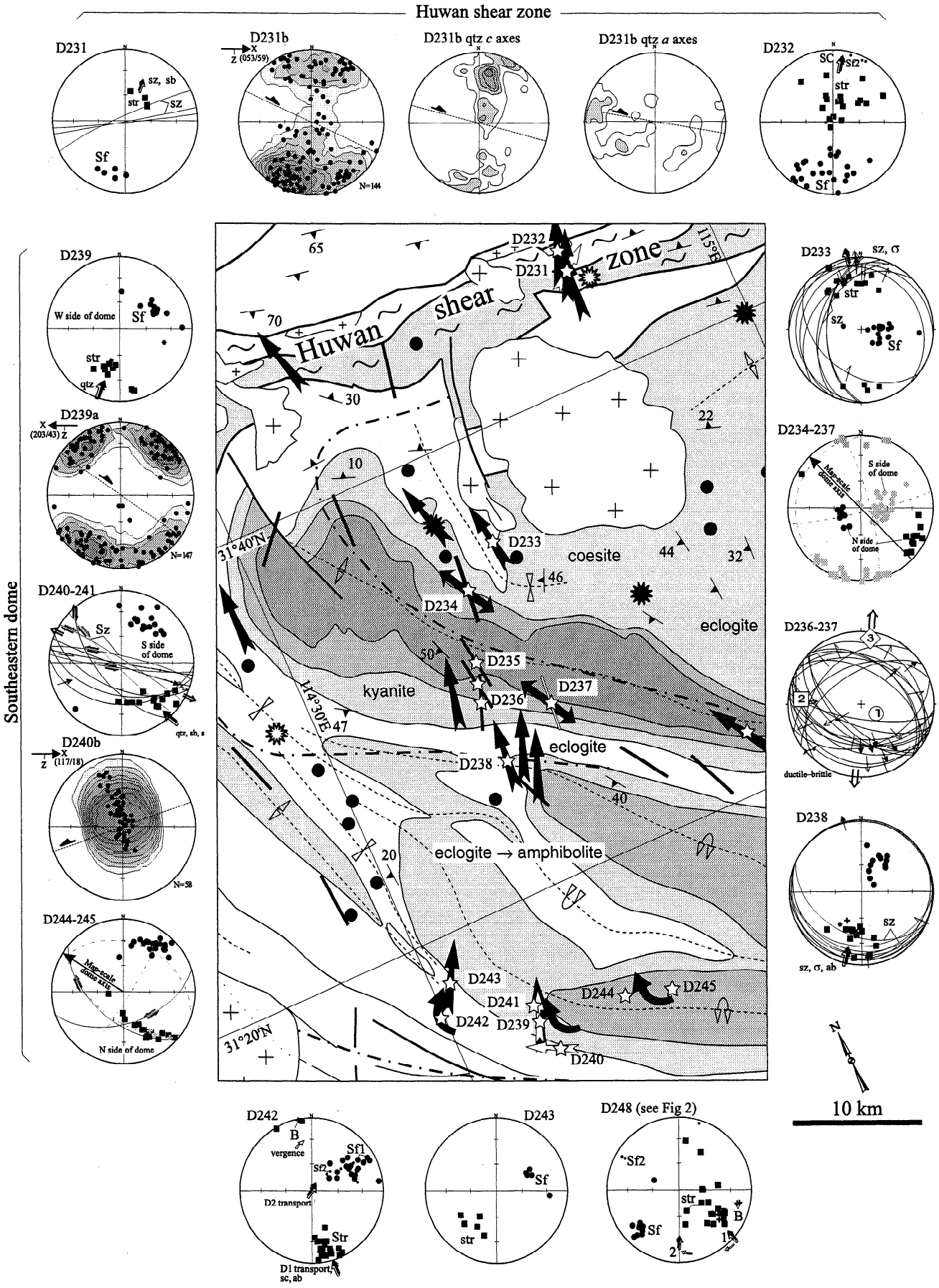

Figure 9. Structural data from northern Hong'an. See caption of Figure 5. Unlabeled data are from *Webb et al.* [2000].

flattening, plane, and constrictional geometries. Furthermore, local or regional constriction of a subhorizontal, layered slab does not provide a simple explanation for the consistent NE fold vergence. We propose that the large-scale Hong'an–Dabie folds resulted from progressive northwestward shearing of a layered crustal slab that initially dipped north. The folds thus formed parallel to the flow direction under overall plane strain and with a NE vergence due to the dip of the slab. We further propose that this folding, a result of shearing of initially dipping competent layers, was amplified by orogen-perpendicular contraction coeval with exhumation. The exhuming slab experienced an overall transpression and an overall constrictional strain.

4.9. Kinematics

The emplacement of the UHP–HP rocks of Hong'an–Dabie occurred by top-NW motion during penetrative strain. Such large-scale deformation has been interpreted commonly in terms of isochoric plane strain, i.e., ideal simple shear and pure shear. Vorticity analysis in various tectonic environments, however, indicates that these ideal strain regimes are rare in nature. If exhumed under a general shear with the shortening axis of the pure shear component subperpendicular to the simple shear plane, the UHP–HP slab could have elongated parallel to the shear plane, thinned vertically, and stretched along the shear plane.

Extensional shear bands, asymmetric boudinage, and foliation-breaking shear zones are ubiquitous in Hong'an–Dabie (Figures 4–9), and formed during and after the development of the regional foliation. The development of shear bands is still not completely understood, but they generally occur in anisotropic rocks and partition flow into domains dominated by either coaxial or noncoaxial flow [e.g., *Platt and Vissers*, 1980; *Platt*, 1984]. In isotropic rocks, two sets of conjugate shear bands/zones are expected in a general flow field. In a general noncoaxial deformation one of the shear band sets makes a smaller angle with the foliation than the other, and both the material anisotropy (i.e., the mylonitic foliation) and the rotation into an unfavorable orientation for continued slip inhibit or weaken the development of the steeper set. If the rock between the shear bands is relatively rigid during shear band/zone formation (as is common during late-stage deformation), it rotates antithetically while the shear-zone wall rock extends parallel to the zone [e.g., *Passchier and Trouw*, 1996].

The development of conjugate shear bands/shear zones and symmetrical boudinage in the Hong'an–Dabie rocks demonstrates that the flow was partitioned by normal shear zones that thinned the rocks vertically and extended them parallel to the movement direction; this interpretation is supported by the presence of documented pressure gaps within the metamorphic sequence [*Carswell et al.*, 1997]. The predominance of single sets of shear bands/zones, the dominance of top-NW shear and asymmetric boudinage, suggests that flow partitioning did occur, and that the flow was intermediate between pure and simple shear. In any case, the presence of these structures in Hong'an–Dabie indicates that the shortening direction must have been relatively steep with respect to the overall deformation zone and that this zone underwent extension along the movement direction.

5. Geochronology

Important constraints on the history of the UHP rocks are provided by U/Pb zircon dating and $^{40}Ar/^{39}Ar$ dating of hornblende, K-white mica (henceforth "muscovite"), biotite, and K-feldspar. Our earlier geochronologic work in the Dabie area was reported by *Hacker and Wang* [1995] and *Hacker et al.* [1995, 1998], and work in Hong'an was presented by *Webb et al.* [1999].

5.1. U/Pb Zircon Ages

New U/Pb zircon ages were obtained on five samples (Figure 10 and Table 2; complete data are available from the World Wide Web server for the Department of Geological Sciences, University of California, Santa Barbara, node at http://www.geol.ucsb.edu/~hacker/suppleData/UHPTriassic) using the sensitive high-resolution ion microprobe (SHRIMP) II at Australian National University, following procedures of *Muir et al.* [1996]. Previous SHRIMP and thermal-ionization mass spectrometry (TIMS) [*Ames et al.*, 1996; *Rowley et al.*, 1997; *Xue et al.*, 1997; *Hacker et al.*, 1998] identified that most zircons from Dabie have Precambrian cores that range from ~625 to 800 Ma, the two most precise such ages are 756.6 ± 0.8 Ma [*Xue et al.*, 1997] and 772.5 ± 9.5 Ma [*Rowley et al.*, 1997]. Four of the samples dated in this study also have Precambrian cores or are wholly Precambrian. Specifically, nine of ten grains from orthogneiss DS253 yielded a mean age of 778 ± 7 Ma, and two grains from DS236 have a mean age of 779 ± 12 Ma. DS43 and DS337 yielded a broader range of ages, with peaks at ~660 Ma and ~735 Ma, similar to zircons analyzed by *Hacker et al.* [1998]. Such rocks were likely derived from the Yangtze craton, which has a distinctive ~750 Ma signature [*Rowley et al.*, 1997; *Hacker et al.*, 1998]. This provides further support to the idea that the exhumed Yangtze craton extends as far north as the Luzhenguang and Foziling Groups in Dabie and the Huwan Formation in Hong'an [*Hacker et al.*, 1998].

Many Dabie–Hong'an zircons have yielded Triassic ages, either SHRIMP ages from rims or TIMS lower intercept ages. Precise ($2\sigma \leq 2.5$ Ma) Triassic TIMS ages from four Dabie eclogites or associated UHP gneisses are all 218.5 Ma [*Ames et al.*, 1996; *Rowley et al.*, 1997]. Eclogites from two localities have given Sm/Nd ages concordant with this, at 225 ± 7 Ma [*Chavagnac and Jahn*, 1996] and 221 ± 5 Ma [*Li et al.*, 1993]. Together, these data have been taken to imply that the UHP metamorphism happened at 218.5 Ma. Eight of ten grains from our sample DS347B have a mean age of 215 ± 5 Ma (2σ), concordant with the 218.5 Ma TIMS ages. However, in the five samples studied by SHRIMP that have yielded Triassic ages [*Hacker et al.*, 1998; *Maruyama et al.*, 1998], there is a peak in ages around 218.5 Ma, but the ages actually cover a broad range from 205 ± 5 Ma to 248 ± 7 Ma (histogram in Figure 10). We [*Hacker et al.*, 1998] proposed that the 218.5 Ma event might reflect post-UHP zircon growth and that the UHP event might be as old as ~240 Ma, on the basis of these data and two Sm/Nd ages from Dabie of 246 ± 8 Ma (garnet–clinopyroxene (gar–cpx) eclogite, *Okay et al.* [1993]) and 244 ± 11 Ma (gar–cpx–whole rock pyroxenite, *Li et al.* [1993]). The data collected in this study do not refute this hypothesis, and also serve to emphasize the possibility of zircon growth as young as 205 Ma.

The implications of zircons as old as ~240 Ma affect an area broader than the Dabie Shan. For example, the Songpan–Ganze flysch (Figure 1) is considered to have been derived from the Dabie Shan, beginning in Anisian and continuing through the Norian (~240-210 Ma, *Nie et al.* [1994] and *Zhou and Graham* [1996]). *Bruguier et al.* [1997] tested this hypothesis by dating detrital zircons from the Songpan–Ganze flysch; they concluded that the absence of 219 Ma zircons in the Songpan–Ganze flysch

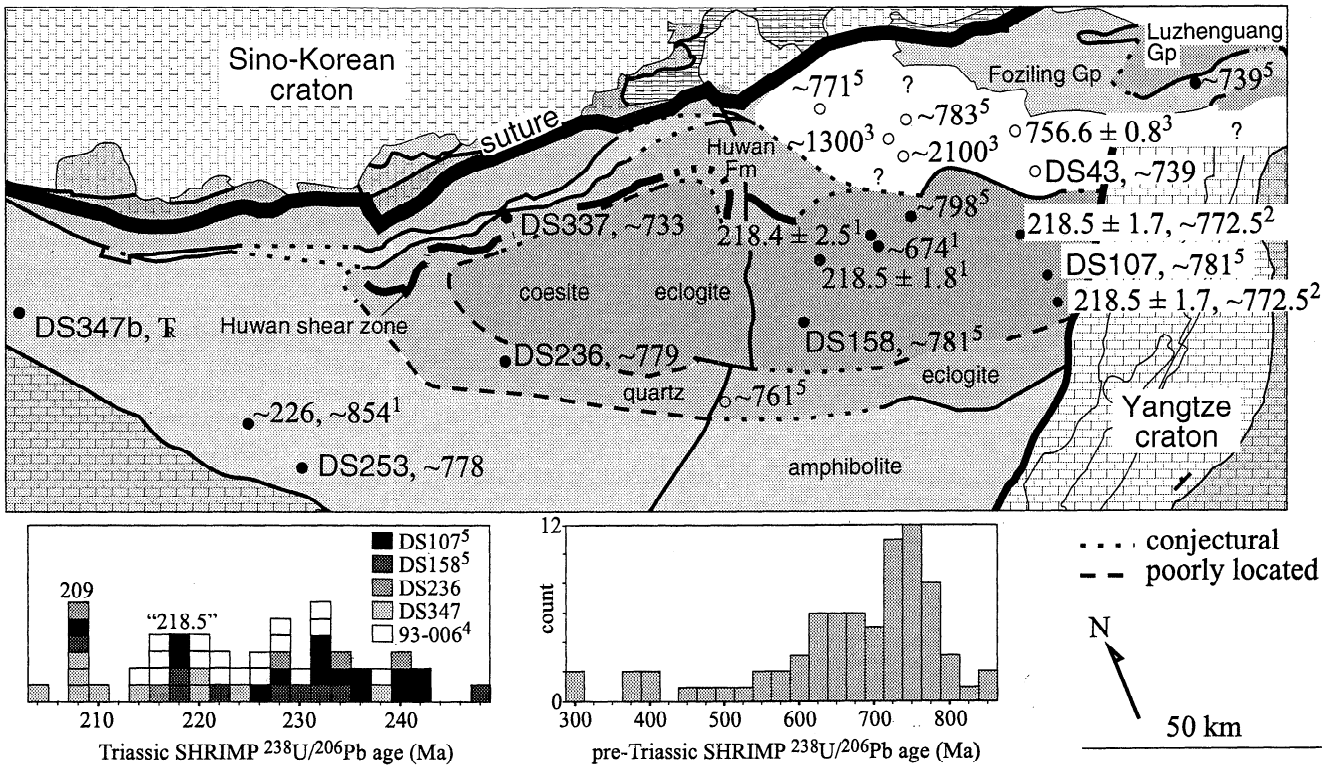

Figure 10. Zircon ages (Ma) from the Dabie–Hong'an area shown on pre-Cretaceous palinspastic restoration of *Hacker et al.* [1998]. Open circles denote samples whose pre-Cretaceous location is speculative. At localities where more than one age has been published, only the more precise age is shown. Histograms show Triassic and older SHRIMP ages from this study, *Hacker et al.* [1998], and *Maruyama et al.* [1998]; 1σ uncertainties are generally ±3 Ma (DS107, DS158) and ±6 Ma (DS236, DS347, 93-006). Superscripts indicate source: 1, *Ames et al.* [1996]; 2, *Rowley et al.* [1997]; 3, Xue et al. [1997]; 4, *Maruyama et al.* [1998]; and 5, *Hacker et al.* [1998].

Table 2. Geochronology Sample Descriptions and Locations

Sample	Stop	Rock	N Latitude	E Longitude
DS1	D1	granite cobble in Upper Cretaceous Sanjanpu Formation sediment	30°41.65'	115°54.05'
D32	D32	detrital ksp Upper Cretaceous Xiafuqiao Formation red bed	31°21.53'	116°22.17'
DS43	D30	gar-bio schist in Foziling	31°21.53'	116°22.17'
DS48	D35	mus schist in Luzhenguang	31°18.01'	116°30.15'
DS51	D36	gabbroic gneiss in Luzhenguang	31°16.42'	116°28.22'
DS52	D36	deformed granitic dike in Luzhenguang	31°16.42'	116°28.22'
DS54	D36	weakly ductilely and brittlely deformed gabbrodiorite	31°15.55'	116°27.38'
DS84	D67	UHP paragneiss near Wuhe	30°49.19'	116°13.32'
DS99	D74	mus segregation in UHP paragneiss west of Qianshan	30°40.04'	116°29.13'
DS101	D74	qtz-bio-ksp vein in UHP paragneiss west of Qianshan	30°40.04'	116°29.13'
DS105	D74	mus segregation in UHP paragneiss west of Qianshan	30°40.04'	116°29.13'
DS106	D75	bio-ksp-qtz segregation in UHP gneiss NW of Shima	30°32.48'	116°17.01'
DS108	D75	mus segregation in UHP paragneiss NW of Shima	30°32.48'	116°17.01'
DS109	D75	mus segregation in UHP eclogite NW of Shima	30°32.48'	116°17.01'
DS110	D75	UHP bio paragneiss NW of Shima	30°32.48'	116°17.01'
DS120	D76	bio-ksp-qtz-sph-ep vein in UHP gneiss	30°29.33'	116°18.14'
DS123	D79	granitic orthogneiss south of Queyeling	30°24.18'	116°07.16'
DS129	D79	micaceous quartzite south of Queyeling	30°24.18'	116°07.16'
DS135	D81	qtz-bio-mus veins in amphibolite	30°21.44'	115°59.29'
DS136	D82	qtz-bio-mus veins in amphibolite	30°21.80'	115°59.75'
DS137	D83	gar amphibolite	30°21.02'	116°00.28'
DS138	D84	HP paragneiss	30°20.42'	116°00.29'
DS220a	D220	detrital ksp Paleocene Hongqiao Formation red beds	31°28.38'	116°34.75'
DS236	D236	bio quartzofeldspathic orthogneiss	31°30.09'	114°39.62'
DS244b	D244	bio quartzofeldspathic vein	31°14.06'	114°38.45'
DS247a	D247	orthogneiss in SW Dabie	30°49.27'	114°56.13'
DS253	D253	mus quartzofeldspathic orthogneiss	31°28.70'	114°06.55'
DS337	D337	bio quartzofeldspathic orthogneiss	31°45.20'	114°47.90'
DS347B	D347	bio quartzofeldspathic orthogneiss with mafic layers	32°00.60'	113 43.60'

Here, bio, biotite; ep, epidote; gar, garnet; mus, K-white mica; qtz, quartz; and sph, sphene.

implies that the Dabie Shan cannot have been the source. However, they did find two zircons with U/Pb ages of 233 ± 1 and 231 ± 1 Ma, within the range of our new zircon ages, implying that the Dabie Shan probably was the source of the flysch after all.

5.2. $^{40}Ar/^{39}Ar$ Ages

Our new $^{40}Ar/^{39}Ar$ spectra are presented in six plots in Figure 11; data are summarized in Table 3 and given in detail at http://www.geol.ucsb.edu/~hacker/suppleData/UHPTriassic, and analytical procedures are given by *Hacker et al.* [1996]. Only three spectra yielded plateau ages, while two additional spectra are flat but not strictly plateaux (Figure 11a). Four spectra are staircase shaped (serially increasing step ages) (Figure 11b). The majority of the spectra show excess ^{40}Ar (Figures 11c–11e) typical of HP rocks [*Scaillet*, 1998].

5.3. $^{40}Ar/^{39}Ar$ Hornblende Ages

All hornblende spectra that we have collected (locations in Figure 2), other than DS51 and DS54, show inhomogeneously released excess ^{40}Ar; this is most clearly evident in high-precision

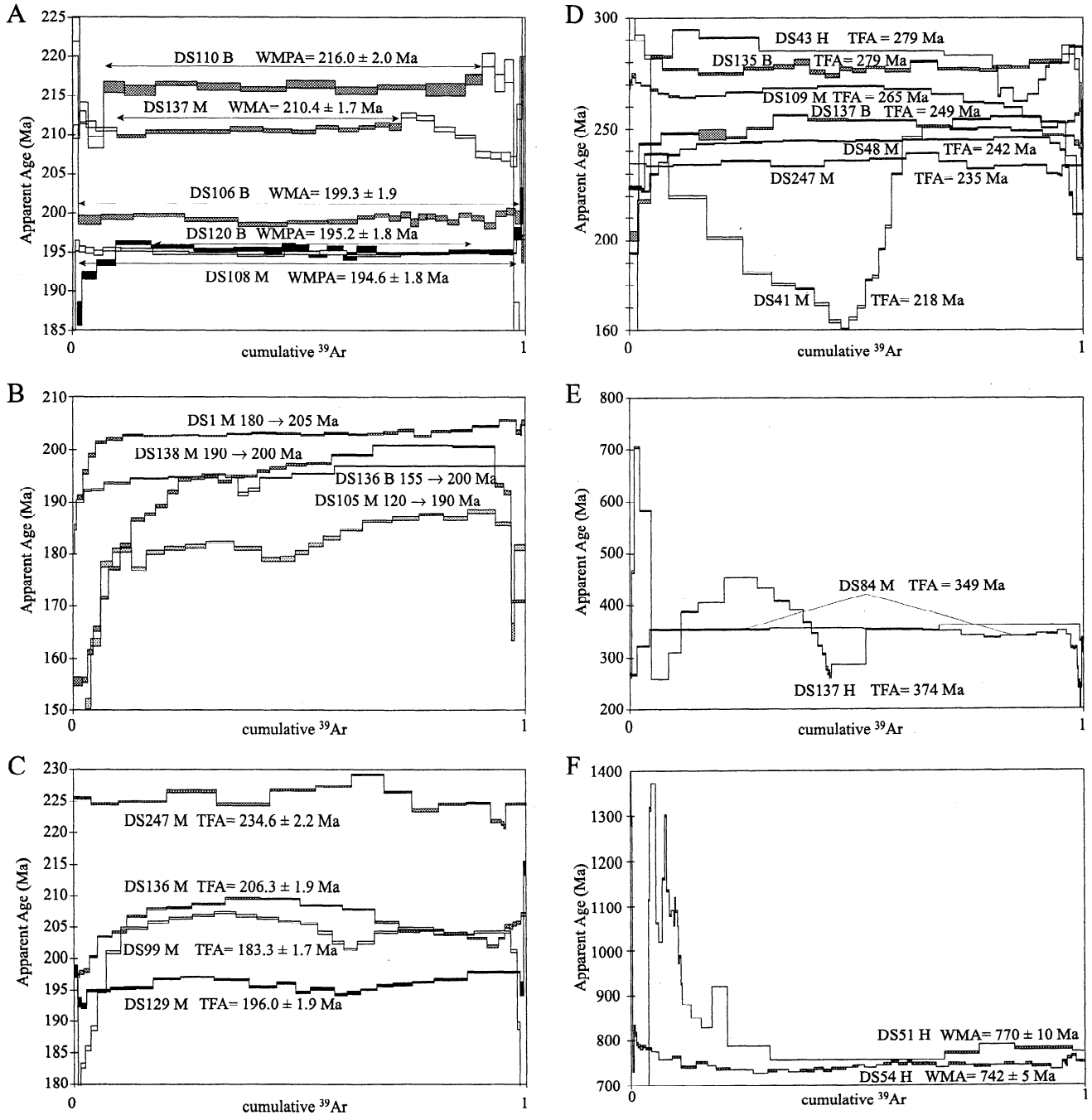

Figure 11. New $^{40}Ar/^{39}Ar$ spectra. (a) Spectra with plateau ages. (b) Staircase-shaped spectra, interpreted as the result of slow cooling or reheating. (c–e) Spectra influenced by excess ^{40}Ar. (f) Spectra showing circa 750 Ma Precambrian ages. WMPA, weighted mean plateau age; WMA, weighted mean age; TFA, total fusion age.

Table 3. Summary of $^{40}Ar/^{39}Ar$ Data

Sample	Mineral	J	Weight, mg	Grain Size, μm	Interpretation
D32	ksp	0.004518	9.0	400	117–128 Ma and Triassic
DS52	ksp	0.004613	6.5	400	180 ± 10 Ma cooling
DS101	ksp	0.003610	12.7	400	initial cooling prior to 175 Ma; reheating and cooling at 140 ± 10 and 90 ± 10 Ma
DS106	ksp	0.003628	11.0	400	initial cooling prior to 170 Ma; reheating and cooling at 90 ± 20 Ma
DS120	ksp	0.003593	8.5	400	initial cooling prior to 190 Ma; reheating and cooling at 90 ± 10 Ma
DS123	ksp	0.004615	2.7	400	initial cooling at ~205 Ma; reheating at 150 ± 10 Ma and cooling at 90 ± 10 Ma
D220a	ksp	0.004550	7.0	400	117–128 Ma and Triassic
D244b	ksp	0.004561	7.3	400	initial cooling at >170 Ma; reheating and cooling 150 ± 20 Ma and 120 ± 10 Ma
D247a	ksp	0.004565	8.4	400	initial cooling prior to 150 Ma; reheating and cooling at 135 ± 15 and 95 ± 10 Ma
D249c	ksp	0.004592	5.8	400	initial cooling at >170 Ma; reheating and cooling 130 ± 5 Ma

Sample	Mineral	J	Weight, mg	Grain Size, μm	TFA, Ma	IA, Ma	MSWD	$^{40}Ar/^{36}Ar$	WMPA, Ma	Steps Used	$\%^{39}Ar$ Used
DS1*	mus	0.004611	2.5	400	202.5 ± 1.9	na	na	na	180 → 205	na	na
DS43	mus	0.003699	2.7	400	218.0 ± 2.1†	na	na	na	na	na	na
DS43	hbl	0.004494	12	175	279.5 ± 2.6†	na	na	na	na	na	na
DS48	mus	0.004610	1.9	75	241.9 ± 2.3†	na	na	na	na	na	na
DS51	hbl	0.004529	25	200	789.1 ± 6.4	na	na	na	770 ± 10†‡	26–31/31	69
DS54*	hbl	0.004183	8.6	200	749.2 ± 1.3	na	na	na	742 ± 5†‡	18–62/62	78
DS84	mus	0.003669	2.7	400	348.8 ± 0.3†	na	na	na	na	na	na
DS99	mus	0.004612	3.1	400	183.4 ± 1.7	na	na	na	183.3 ± 1.7†‡	8–24/27	74
DS105	mus	0.004606	2.2	350	175.5 ± 1.7	na	na	na	120 → 190†	na	na
DS106	bio	0.003622	2.0	300	200.4 ± 1.9	na	na	na	199.3 ± 1.9†‡	2–26/26	99
DS108	mus	0.004601	1.8	400	194.7 ± 1.8	194.6 ± 1.8	1.0	303 ± 19	194.6 ± 1.8†	9–15/16	55
DS109	mus	0.004609	2.1	300	264.9 ± 2.5†	na	na	na	na	na	na
DS110	bio	0.003717	1.7	200	214.9 ± 2.0	215.7 ± 2.0	0.48	344 ± 20	216.0 ± 2.0†	4–13/18	84
DS120	bio	0.003588	2.6	200	194.7 ± 1.8	195.2 ± 1.8	1.0	289 ± 17	195.2 ± 1.8†	7–18/21	71
DS129	mus	0.004604	2.6	400	196.0 ± 1.9†	na	na	na	195.9 ± 1.9‡	5–25/27	96
DS135	bio	0.003655	4.3	400	278.5 ± 2.6†	269.3 ± 3.2	1.0	1641 ± 591	na	4–23/27	92
DS136	bio	0.004605	3.3	100	195.1 ± 1.9	na	na	na	155 → 200†	na	na
	mus	0.004599	3.5	175	206.3 ± 1.9†	na	na	na	208 ± 1‡	na	na
DS137	bio	0.004594	1.3	150	249.5 ± 2.3†	na	na	na	na	na	na
	hbl	0.004598	11.3	150	373.9 ± 3.4†	na	na	na	na	na	na
	mus	0.004605	1.5	100	210.4 ± 2.0	210.7 ± 2.0	1.7	274 ± 7	210.4 ± 1.7†‡	5–15/25	63
DS138	mus	0.004597	2.0	175	189.3 ± 1.8	na	na	na	190 → 200†	na	na
D247a	mus	0.004042	0.9	200	234.6 ± 2.2	na	na	na	234.2 ± 2.2†‡	na	na

Hbl, hornblende; bio, biotite; mus, K-white mica; J, irradiation flux parameter; TFA, total fusion age (uncertainty reflects only analytical precision); IA, isochron age; MSWD, mean square weighted deviation [*Wendt and Carl*, 1991] which expresses the goodness of fit of the isochron [*Roddick*, 1978]; WMPA, weighted mean plateau age. Arrows indicate range of ages, as discussed in text. IA and WMPA are based on steps and fraction of ^{39}Ar listed in the last two columns. Complete $^{40}Ar/^{39}Ar$ data are available from the World Wide Web server for the Department of Geology, University of California, Santa Barbara, node at http://www.geol.ucsb.edu/~hacker/suppleData/UHPTriassic.

* Samples run at University of California, Santa Barbara (others run at Stanford University).

† Preferred age.

‡ Not a plateau age, but a weighted mean age whose quoted uncertainty reflects our assessment of the spectrum quality (generally encompassing the range in ages of nearly concordant steps).

spectra such as DS137 (Figure 11c). The spectra are not hump or saddle shaped, but crankshaft shaped, and are not amenable to isochron analysis. All hornblende $^{40}Ar/^{39}Ar$ ages published for Dabie by other authors either are not accompanied by spectra [*Mattauer et al.*, 1991] or are based on low-precision spectra with few steps [*Cao and Zhu*, 1995; *Chen et al.*, 1995]; because all our hornblende spectra include excess Ar, it is likely that these lower precision spectra published by other workers do as well. Thus no $^{40}Ar/^{39}Ar$ or K/Ar hornblende ages from Dabie HP or UHP rocks are reliable. In contrast, samples DS51 and DS54, while not yielding plateau ages, yield high-precision spectra that suggest closure near ~750 Ma (Figure 11f). Both of these samples come from metaplutonic rocks of the Luzhenguang Group, and their ~750 Ma hornblende ages indicate that (1) these samples were derived from the Yangtze craton, and (2) temperatures subsequently remained below 500°–600°C.

5.4. $^{40}Ar/^{39}Ar$ Muscovite Ages

More $^{40}Ar/^{39}Ar$ ages from Hong'an–Dabie–Sulu UHP rocks have been obtained on muscovites than any other phase; hence an understanding of their meaning is critical. At first blush, the spectra are complicated, and the geographical distribution of different ages is overwhelming (Figure 12a). To make sense of this, we divide our muscovite spectra, and those of *Eide et al.* [1994], into four categories (Figures 12a and 12b): flat spectra with plateau ages, staircase spectra, hump-shaped spectra with excess ^{40}Ar, and crankshaft-shaped spectra with excess ^{40}Ar. Note that no eclogite from Hong'an–Dabie has yielded an interpretable $^{40}Ar/^{39}Ar$ spectrum of muscovite or any other mineral, presumably because radiogenic ^{40}Ar in minerals in these low-K rocks is swamped by Ar derived from the enclosing K-rich gneiss. All interpretable spectra come from rocks other than eclogite.

The interpretation of flat spectra is straightforward, and we follow other workers in interpreting the low-age ends of hump-shaped spectra as maximum ages for the most recent episode of Ar loss. Staircase spectra are more difficult to interpret. *Grove* [1993] argued that staircase spectra can reflect ^{40}Ar gradients in muscovite crystals if H_2O loss in vacuo occurs by diffusion and not by recrystallization or delamination. Staircase spectra might thus, in favorable cases, result from (1) faithful in vacuo degassing

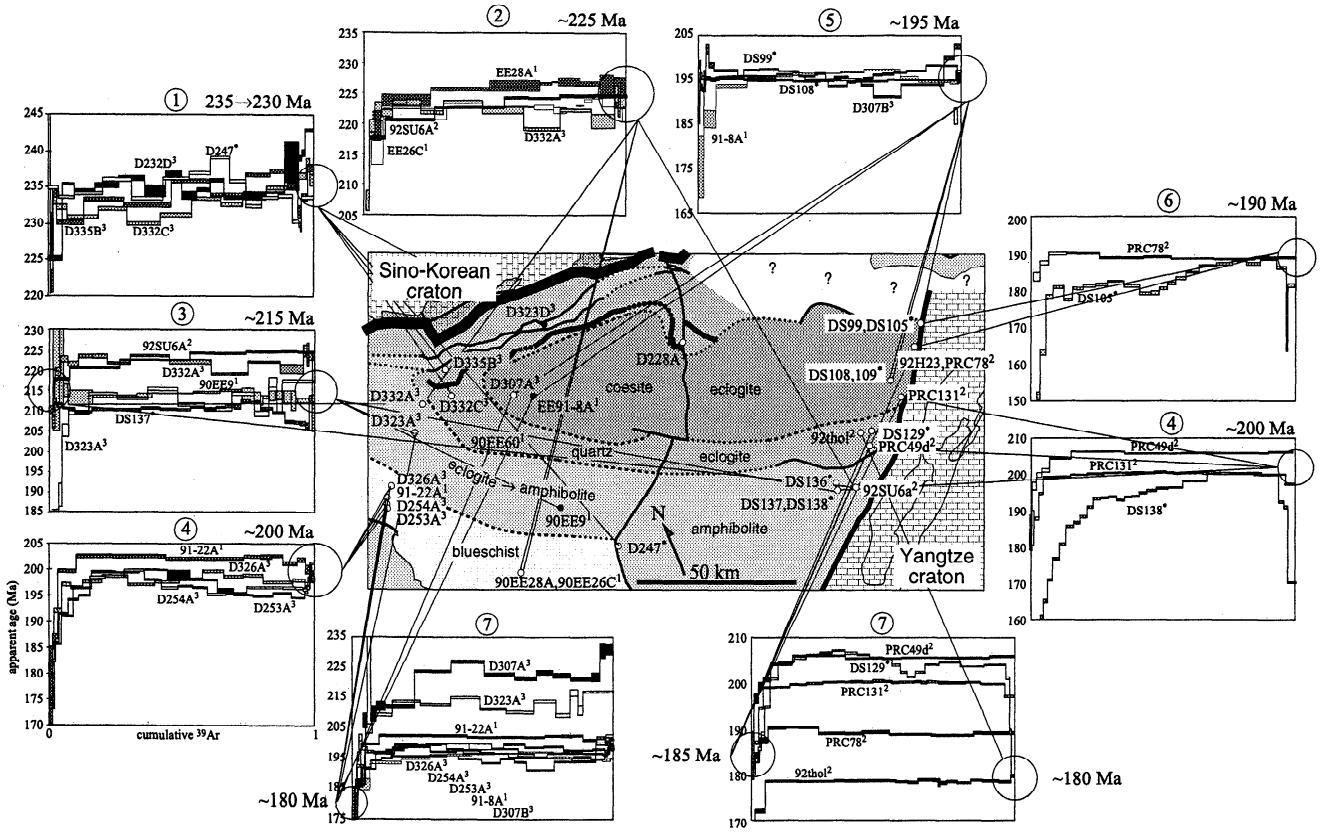

Figure 12a. K-white mica $^{40}Ar/^{39}Ar$ ages from the Dabie–Hong'an area shown on pre-Cretaceous palinspastic restoration of *Hacker et al.* [1998]. Superscripts indicate source: 1, *Eide et al.* [1994]; 2, *Hacker and Wang* [1995]; 3, *Webb et al.* [1999]; and asterisk, this study. Spectra with staircase shapes may appear twice, once corresponding to their oldest step age and once corresponding to their youngest step age. Vertical axes are apparent age (Ma); horizontal axes are cumulative ^{39}Ar released.

of ^{40}Ar zoning produced by protracted crystal growth, (2) faithful in vacuo degassing of ^{40}Ar zoning in crystals produced by diffusive loss in Earth, or (3) differential in vacuo degassing of a population of mixed younger, less retentive (e.g., smaller) grains or domains and older, more retentive (e.g., larger) grains or domains.

In support of case 1, extremely fine grained (2–6 μm) neocrystallized muscovites from the basal mylonite of the Morcles nappe, Switzerland, yielded staircase spectra whose low- and high-T step ages match independent determinations of the duration of thrusting [*Kirschner et al.*, 1996]. In support of case 2, *Grove and Bebout* [1995] found that Catalina Schist muscovites coarser than 250 μm yielded plateaux while finer grained muscovites yielded staircase spectra whose high-T age steps are similar to the plateaux ages; the absence of growth/recrystallization textures in the fine-grained mica led Grove and Bebout to interpret these gradients as the result of diffusive loss. In favor of case 3, *Hames and Cheney* [1997] used laser spot ages to show that a 425°–525°C metamorphic overprint produced new fine-grained muscovites with ages reflecting the time of the overprint and caused Ar loss in older porphyroclasts only where the porphyroclasts were recrystallized; bulk heating of muscovites from such a rock could yield staircase spectra.

Which, if any, of these interpretations might be correct for the muscovites from Dabie and Hong'an? Figure 12b shows compositions we determined for muscovites with different types of spectra. The different Si and Ti compositional types (labeled A, B, C, D, and E in inset to Figure 12b) are interpreted to represent a metamorphic sequence from HP, high-Si crystals (type A) to low-P, low-Si crystals (type E), following the white mica compositional variation detailed by *Guidotti and Sassi* [1998]. Each of these compositional types is now discussed in detail. Two blueschist samples contain only type A unzoned high-Si phengites; both of these spectra are staircase shaped, but span < 5 m.y. The low metamorphic T (350°–450°C) for these samples suggests that the staircase spectra reflect protracted growth at 220–227 Ma below the closure temperature. Type B muscovites, from three samples of the eclogite → amphibolite unit, all have high Si contents; some of the crystals are zoned. Temperatures in this unit were at least partly above closure, and we interpret the low-T end of both spectra to reflect final closure at 212–215 Ma. Type C muscovites, in four samples, show an extensive range of Si contents, with all crystals showing zoning. Three of these samples experienced peak T in excess of closure temperature, and two of those show a range of ages from 185 to 205 Ma, which we interpret as closure ages. Four samples from the coesite-eclogite unit have type D unzoned high-Si muscovites and unzoned low-Si muscovites; these low-Si crystals are also the first with high Ti. These features indicate two periods of growth, and the spectra from these samples must be a mixture of the two sets of grains. Tentatively, we assume that the HP event is >198 Ma and the low-P event is <189 Ma. Two samples contain only type E muscovites

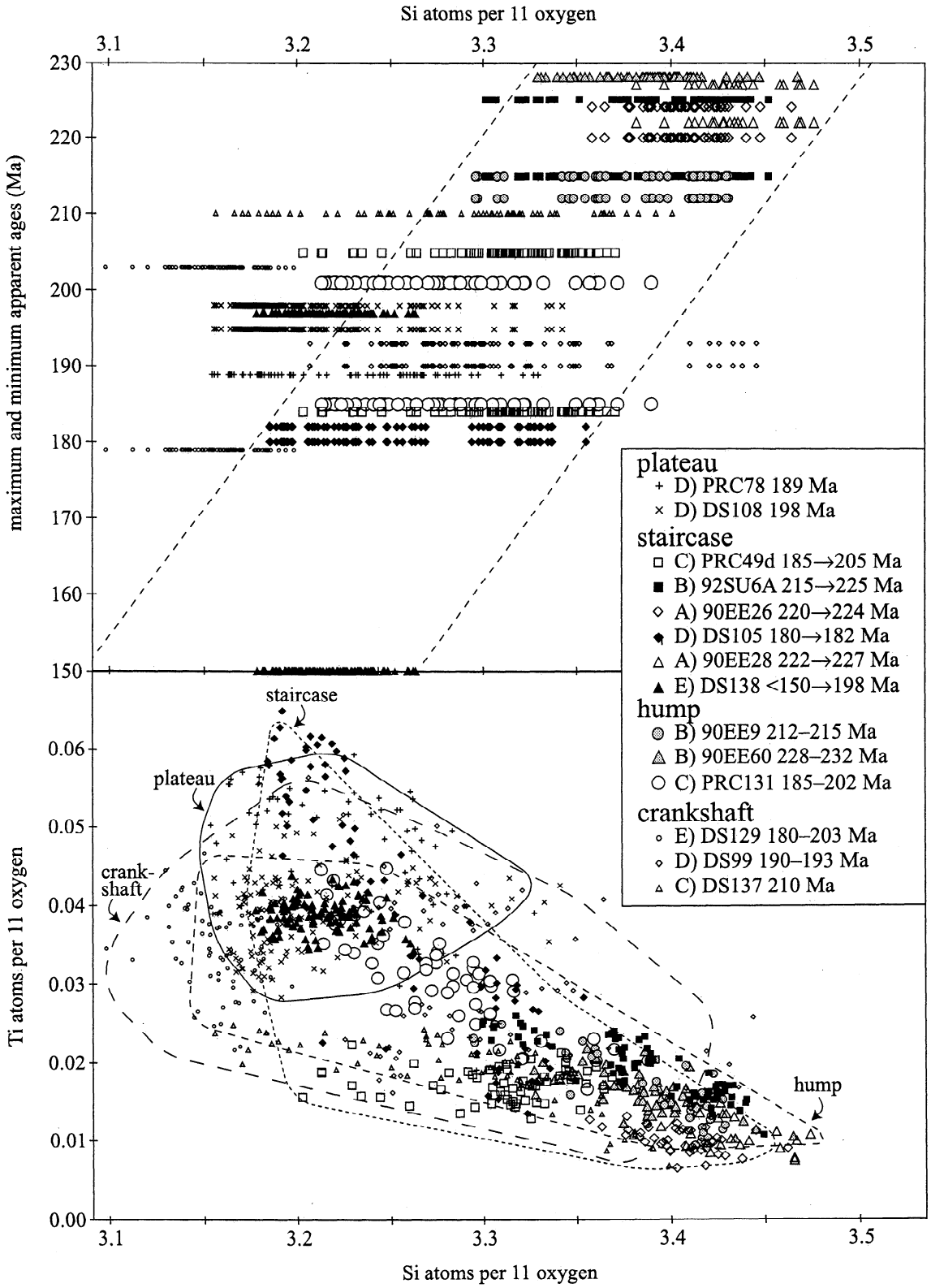

Figure 12b. Do muscovite compositions determined by electron probe microanalysis correspond to different types of $^{40}Ar/^{39}Ar$ spectra? (top) Muscovite Si contents show a correlation with both minimum and maximum step ages of spectra. (bottom) Spectrum types show weak differences in Si and Ti contents.

low in Si, suggesting that vestiges of any HP event have been erased. Again, the HP event is probably >203 Ma, and the low-P event is <180 Ma. In summary, the oldest samples we probed show unzoned high-Si, low-Ti muscovites and imply protracted growth at 220–227 Ma. The youngest samples have unzoned low-Si, high-Ti crystals, and probably closed by 180 Ma. Intermediate samples have intermediate ages, but it is hard to assign specific meaning to them. These data demonstrate that spectrum shape is a poor indicator of meaning, but that compositional data aid in interpreting the spectrum shapes from HP and UHP muscovites.

Muscovite data from the Dabie–Hong'an area can thus be placed in seven groups, based on age and spectrum type (Figure 12a). The oldest samples form a group (group 1) with ages from 230–235 Ma; four of these samples are located along the Huwan shear zone along the northern edge of Hong'an, which was thus the first part of Hong'an to cool below 400°–500°C (muscovite closure temperatures inferred by *Kirschner et al.* [1996] and *Hames and Cheney* [1997]. The next younger group of ages (group 2), ~225 Ma, occur only within the blueschist and amphibolite units and, at least within the blueschist unit, represent crystallization ages. Within the amphibolite unit, spectra are staircase shaped or flat (group 3) suggesting final closure at 210–215 Ma. Three samples from Dabie and four from Hong'an comprise a distinct group (group 4) of staircase spectra with high-T ages of 200–205 Ma and low-T ages of 180–185 Ma. If the Si and Ti data presented above can be generalized to this entire group, the 200–205 Ma ages are minima for HP recrystallization, the 180–185 Ma ages are maxima for low-P recrystallization, and the two groups represent the closure of less and more retentive domains respectively. A similar interpretation applies to samples with ages of 190–195 Ma (groups 5 and 6), which are restricted to the coesite-eclogite unit. The 180–185 Ma, low-T ages of group 4 are a subset of a larger group of geographically widespread samples (group 7).

5.5. $^{40}Ar/^{39}Ar$ Biotite Ages

There are 10 pre-Cretaceous biotite $^{40}Ar/^{39}Ar$ ages from Dabie and Hong'an (Figure 13). The two spectra with oldest ages do not yield plateaux (one is crankshaft shaped and from a pegmatitic vein (PRC104b), the other is hump shaped and from amphibolite (DS137)), and we disregard them. Of the remaining, relatively flat, spectra from paragneisses, five are between 190 and 200 Ma, while the others are 216, 229, and 279 Ma. The coherence among the 190–200 Ma ages, combined with the muscovite ages just discussed, implies that at least the 279 Ma age (DS135) is the result of excess Ar.

5.6. $^{40}Ar/^{39}Ar$ Metamorphic K-Feldspar Ages

Metamorphic K-feldspars (locations in Figure 2) were analyzed to constrain low-T thermal histories. Only two samples yielded spectra suitable for full diffusion-domain analysis [after *Lovera*, 1992] (Figure 14a). DS123 was well fit by histories dominated by initial cooling at ~200 Ma, followed by reheating near 130 Ma. D247a was not well fit by calculated thermal histories but is a pre-Cretaceous rock reheated near 90 Ma. Two K-feldspars, DS106 and DS244B, were not amenable to diffusion-domain analysis because of complexities in their spectra (Figure 14b). Four other samples, DS52, DS101, DS120, and DS249C, were modeled with qualitative cooling histories because the furnace temperature during degassing was not well known.

Most of the spectra have inflections indicating cooling below ~200°C near 170 Ma, though DS106(?), DS120, and DS123 may have been this cool as early as 190 Ma. The spatial distribution of these ages indicates that a large part of Dabie–Hong'an was relatively cold at 170 Ma, and DS123 is particularly important in showing that local areas were cold as early as 200 Ma. Thermal histories for five samples suggest reheating at 130–140 Ma, and histories for four indicate reheating at ~90 Ma (by Cretaceous plutons, *Ratschbacher et al.* [this issue]).

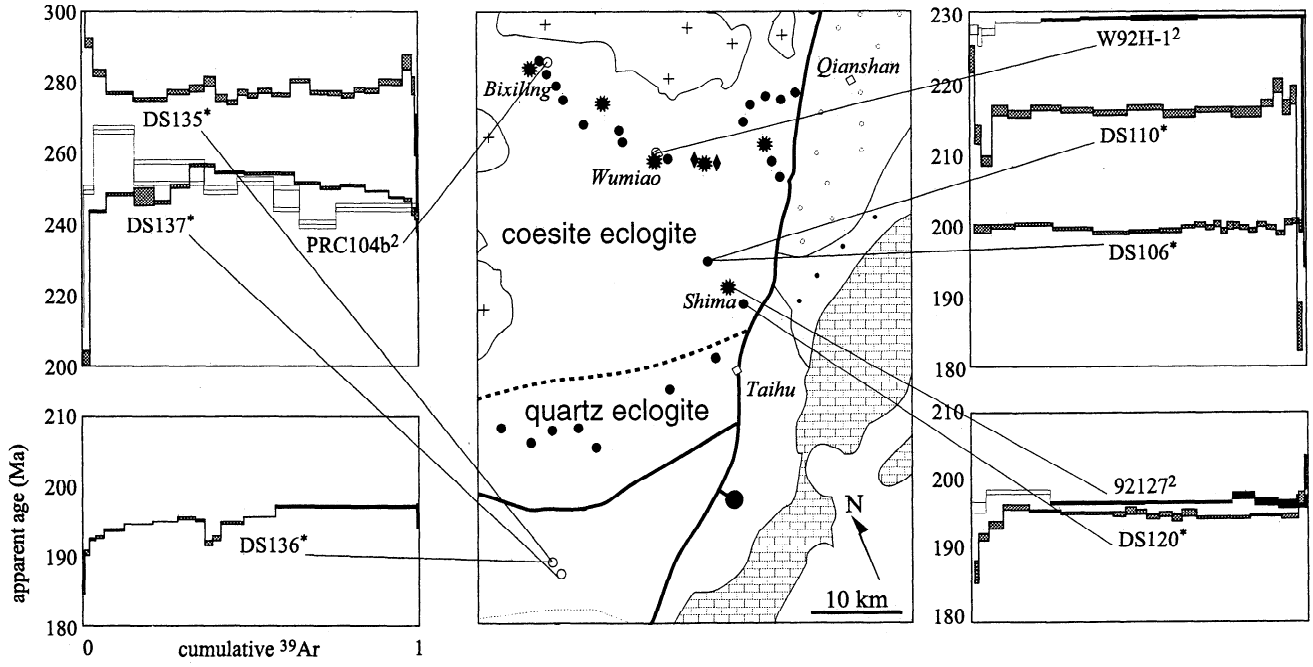

Figure 13. Biotite $^{40}Ar/^{39}Ar$ ages (Ma) from Dabie–Hong'an. Superscripts indicate sources (Figure 12 caption). Vertical axes are apparent age (Ma), and horizontal axes are cumulative ^{39}Ar released.

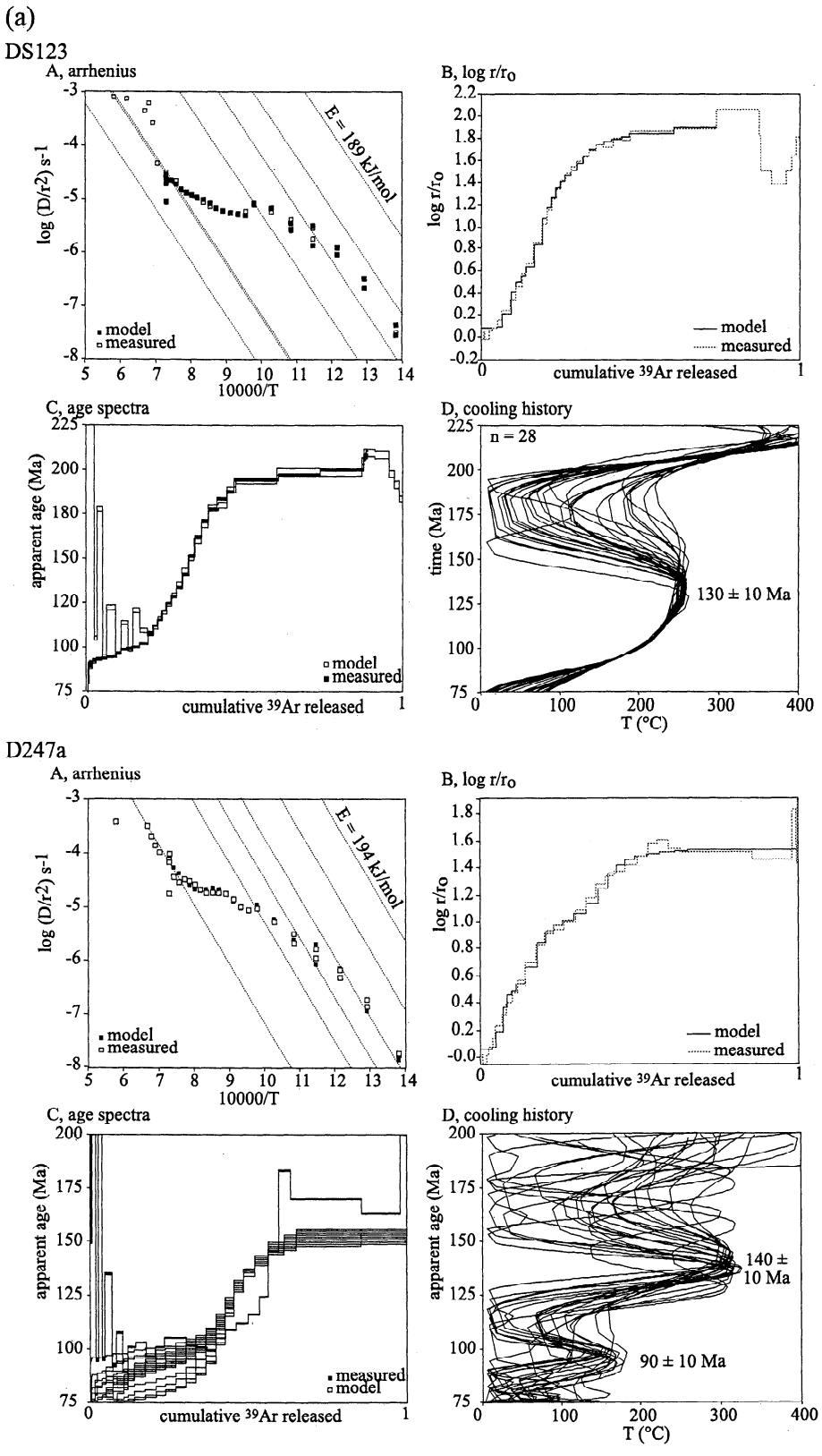

Figure 14. Diffusion-domain analysis of metamorphic K-feldspars. (a) Spectra and quantitative analyses. (b) Spectra and semi-quantitative and qualitative thermal histories.

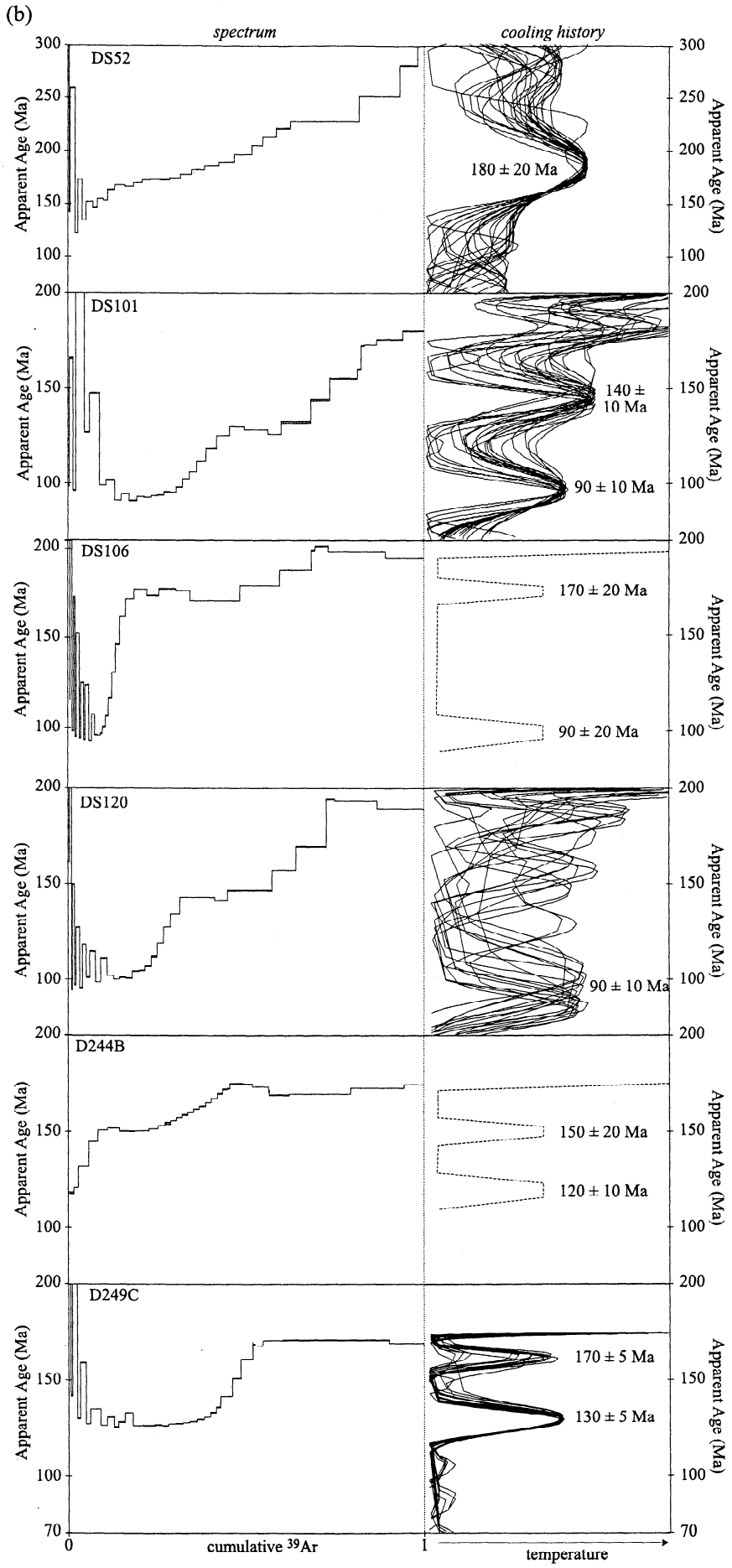

Figure 14. (continued)

5.7. $^{40}Ar/^{39}Ar$ Detrital K-Feldspar Ages

On the north side of Dabie Shan, two red bed localities (D32 and D220a; locations in Figure 2) with detrital K-feldspar grains were sampled to determine the time at which UHP detritus reached the red beds. Neither locality exhibited visible metamorphism, thus we interpret the ages of the grains to date final cooling prior to sedimentary transport. Dozens of centimeter to millimeter size grains were handpicked from the sediment at the outcrop. Five grains from each locality were selected for $^{40}Ar/^{39}Ar$ analysis (Figure 15). To ensure that complex release spectra did not bias our interpretation, each crystal was broken into two fragments and step heated separately with a 6W Ar laser. The expectation was that we would be able to match each crystal half to another half, and, indeed, the isotopic fingerprints of the various grains are relatively distinct. Detrital K-feldspars from locality D32 indicate a maximum depositional age for the red bed of 119 ± 1 Ma, compatible with the assigned depositional age of Late Cretaceous. The source terrane appears to have been dominated by Cretaceous rocks of 123 ± 1 to 119 ± 1 Ma. Relatively low radiogenic yields for some of these feldspars are likely the result of diagenesis. The D220a locality has a maximum depositional age of 123 Ma (middle Early Cretaceous) that also does not conflict with the assigned depositional age of Paleocene.

The abundance of Cretaceous plutonic rocks immediately south of these red beds leaves little doubt as to the source of the Cretaceous grains. Both red bed localities also contain older grains that, in general, yield spectra that begin with ages of 190–220 Ma and climb to ages of 250–280 Ma. Such spectra are compatible with the presence of excess ^{40}Ar, and/or age gradients produced by slow cooling, both are attributes of K-feldspars from the metamorphic core of the orogen (Figure 14). These data do not contain geologically meaningful isochrons, but their isotopic ratios (Figure 15) are compatible with Triassic ages, and the grains were surely derived from the metamorphic core of the orogen.

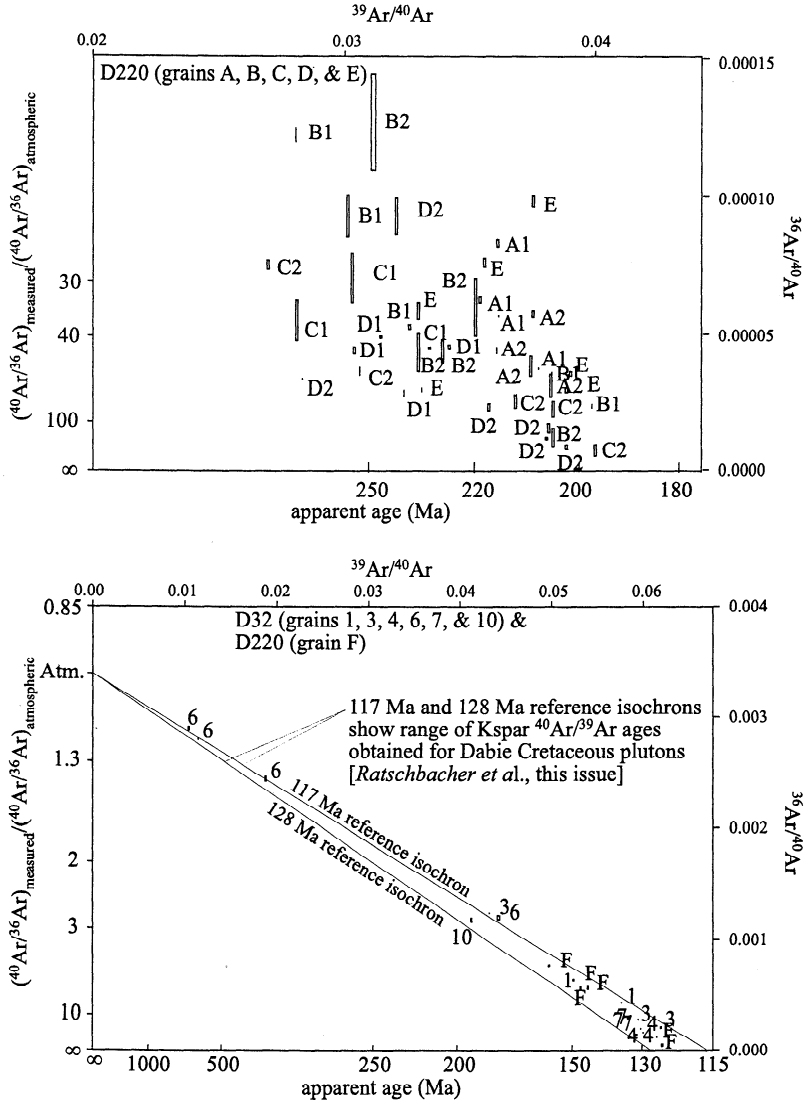

Figure 15. Inverse isochron diagrams [*Roddick*, 1978] for detrital K-feldspars from molassic sediments north of Dabie (locations D32 and D220 in Figure 2). Top and right axis labels are standard; bottom and left axes show apparent age and excess ^{40}Ar as multiples of the atmospheric value, respectively.

6. Discussion

Investigations of the Dabie–Hong'an area are now mature enough to formulate a constrained and testable tectonic model for the exhumation of the UHP rocks.

6.1. Architecture of the UHP Orogen

The unusual shape of the Qinling–Dabie–Sulu suture, with an apparent sinistral offset along the Tan–Lu fault (Figure 1), has been the subject of debate. The suture extends in an ESE arc through the Qinling and then swings more toward the SE in the Dabie area, where the UHP–HP rocks form an eastward widening wedge of progressively higher P rock that is abruptly truncated by the Cenozoic Tan–Lu fault [*Ratschbacher et al.*, this issue]. NE of the belt of Triassic blueschist in the Zhangbaling area the suture has a consistent NE trend defined by UHP rocks in Sulu and HP rocks in the Imjingang belt of Korea [*Ree et al.*, 1996]. Restoring the NW-SE extension across the Hehuai basin, which has up to 8 km of mostly Cretaceous–Paleogene sediments [*Han et al.*, 1989], probably results in a more E–W trending suture in the Qinling–Dabie area, but likely does not bring the Dabie and Sulu structural trends into coincidence. We propose that the southern, passive margin of the Sino–Korean plate was convex toward the SE prior to collision. *Yin and Nie* [1993] explained the left-lateral offset along the Tan–Lu fault as the result of Late Permian and Early Triassic indentation of the Sino–Korean craton by the Yangtze craton. *Gilder et al.* [1999, p. 15,385] have criticized this idea because of a "lack of significant folding of Phanerozoic rocks...north of the Sulu belt" and proposed that the Sino–Korean craton indented the Yangtze craton in the Early to Middle Jurassic instead, leading to paleomagnetically recorded bending of the Yangtze craton fold belt, formation of the Tan–Lu fault, and 70° of relative rotation between the Sino–Korean and Yangtze cratons [*Zhao and Coe*, 1987]. While there is evidence of Cretaceous and Cenozoic strike-slip and normal faulting [*Ratschbacher et al.*, this issue], no well-documented structural data support these ideas of transcurrent Triassic or Jurassic motion along the Tan–Lu fault. In the eastern Dabie foreland, *Schmid et al.* [2000] documented mid-Triassic NW–SE contraction and Late Triassic–Early Jurassic N–S contraction; such deformation implies sinistral shear along a Triassic–Jurassic Tan–Lu fault.

6.2. Exhumation Rate and P–T Path

The P–T history of Dabie–Hong'an rocks during exhumation is partially constrained by the P–T data summarized in Fig 3 and by the thermochronology enumerated in section 5. The UHP rocks were at 825°–850°C and 3.3–4.0 GPa at ~240 Ma and cooled through muscovite closure, probably at crustal depths, by ~200 Ma; they experienced subsequent, perhaps repeated, reheating at amphibolite-facies temperatures and crustal pressures until ~180 Ma. The lower P eclogites along the Huwan shear zone cooled through muscovite closure at 230–235 Ma, the bulk of the quartz eclogites closed by 210–215 Ma, and the blueschists last recrystallized at 220–225 Ma. Such P–T paths, with concomitant decompression and cooling, are only possible if exhumation was rapid or the slab was refrigerated by deeper-level subduction [*Hacker and Peacock*, 1995; *Ernst and Peacock*, 1996]. We can only crudely constrain the rate of exhumation to an order of magnitude rate of >2 mm/yr, a rate that permits a 10 km thick slab to significantly exchange heat with its surroundings. The Barrovian amphibolite-facies overprint was 30–50 m.y. younger, most plausibly reflecting not simple conductive reequilibration following one-stage decompression of the UHP rocks, but subsequent crustal thickening.

6.3. Size of the UHP Slab

Specific bounds can now be placed on the extent of the UHP–HP slab. The UHP–HP rocks, as currently exposed, span ~125 km across strike and ~250 km along strike. Prior to Cretaceous extension these dimensions were closer to ~100 and 200 km, respectively, and updip and along-strike stretching during exhumation means that these are maxima. The present structural thickness of the HP–UHP section in Hong'an, where it can be best assessed, is ~10 km (Figure 2); as argued in section 6.4, this thickness is a minimum because of substantial thinning of the slab during exhumation. No extensive ultramafic rocks have been found at the structurally deepest levels in Dabie or Hong'an, implying that the basal detachment was at or above the Moho. Determining an accurate constraint on the downdip length of the slab hinges on knowing the dip during subduction and the strain during exhumation. Figure 16c shows that a dip of ~45° and downdip length of ~200 km are required if the slab did not thin during exhumation. Because we argue for substantial thinning of the slab during exhumation, 200 km is a maximum; the minimum is constrained by a vertically dipping slab that must reach depths of ~125 km to form diamond.

6.4. Rotation and Deformation of the UHP Slab

Unfolding the "Hong'an antiform", the orogen-scale fold trending NW–SE across Hong'an–Dabie, yields a north dipping lithospheric slab with coesite eclogite in the north and lower P rocks progressively farther south and closer to the interior of the Yangtze craton. The upper boundary of the slab is the Huwan shear zone (Figures 2 and 9), which is immediately south of the suture between the Sino–Korean and Yangtze cratons, implying that it is essentially a plate boundary reactivated as a lithosphere-scale, normal-sense shear zone. The UHP–HP rocks were drawn or driven out from beneath the Sino–Korean craton, imparting a roughly NW–SE stretching lineation and NE-vergent, WNW–ESE trending folds (Figure 16). The UHP–HP rocks comprise the extrusion channel itself and probably underwent a strong coaxial flow component, implying transport-parallel and orogen-parallel elongation within the channel. Strain compatibility requires that the boundaries of the channel were stretching faults [*Means*, 1989].

The westward decrease in depth of exhumation is most easily reconciled with a clockwise rotation of the exhuming slab around a pivot located on the Yangtze craton west or south of Tongbai. This rotation may also be reflected in the clockwise rotation of the stretching lineations within Hong'an and Dabie. The wedge shape of UHP–HP outcrop and the apparent rotation during exhumation imply that the Yangtze craton was subducted to relatively shallow depths in the west and progressively greater depths toward the east.

6.5. Dynamic Exhumation Model

Assume that a Florida-like promontory (Figure 16b) (or a less complex shape; Figure 16a) of the Yangtze craton was subducted beneath the Sino–Korean craton. At some point, the buoyant, subducted continental crust tore away from the oceanic part of the plate and began to rise within the channel between the two cratons (Figure 16c, a la *Chemenda et al.* [1995]). The tear began at the

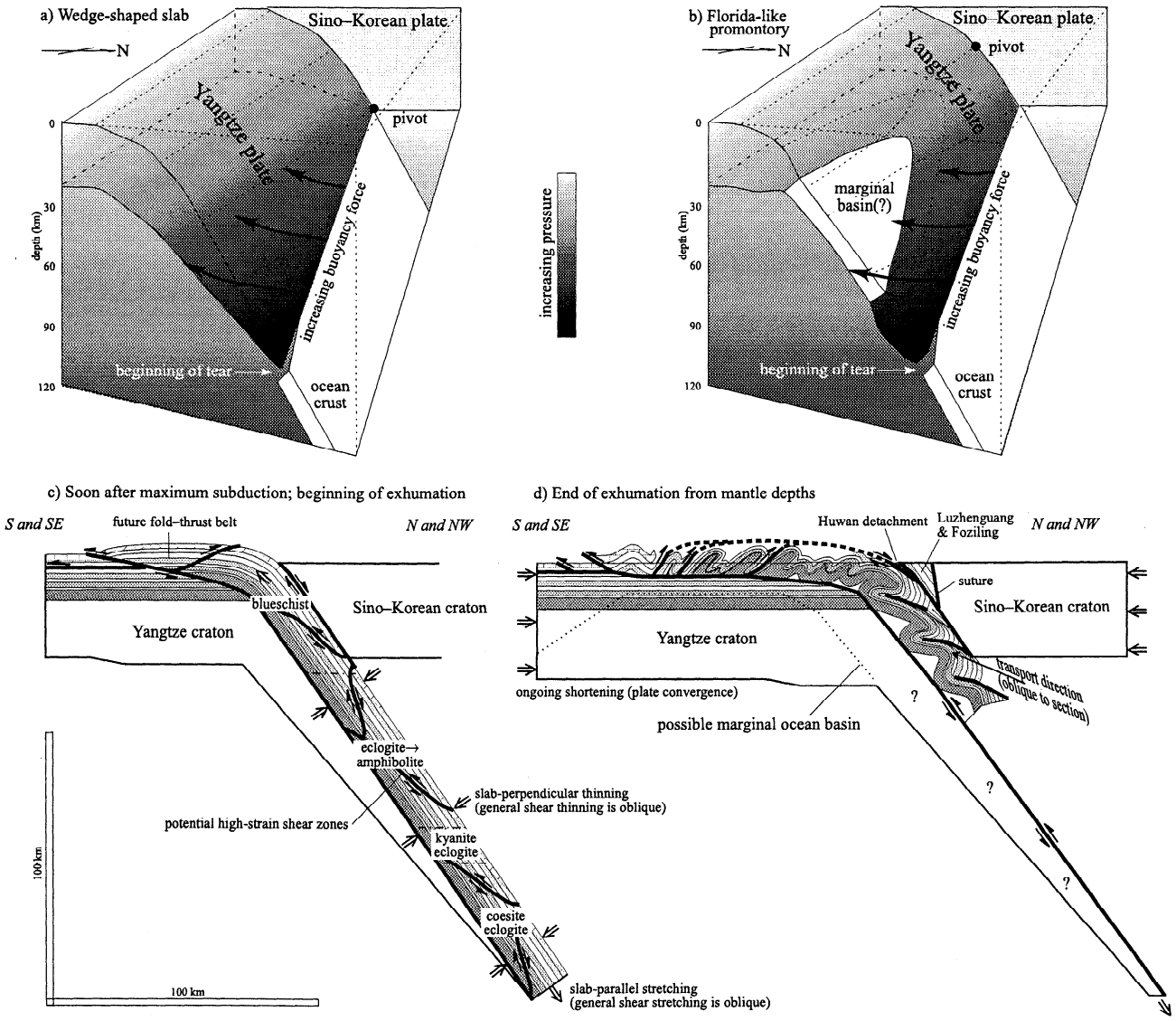

Figure 16. Exhumation of UHP rocks. (a) Subduction of wedge-shaped continental promontory; arrows show pivoting of slab during exhumation. (b) Subduction of Florida-like continental promontory (shaded) attached to oceanic crust (open). (c) Two-dimensional representation of subducted continental crust, with detached sliver beginning to exhume. (d) Two-dimensional representation of continental crust exhumed by buoyancy. (e) Cut-away view of continental promontory exhuming from UHP depths. Strain partitioning induces bulk deep oblique stretching, shallow updip stretching, and slab-orthogonal thinning, along with discrete zones of dextral shear and apparent shortening. Muscovite $^{40}Ar/^{39}Ar$ ages are shown.

deepest point of subduction of buoyant slab and ripped upward along the promontory. The shape and orientation of the subducted crust, combined with the dependence of buoyancy on depth below the Moho, mean that the promontory pivoted about its shallow end, producing an extruded wedge on top of the rest of the Yangtze plate, which could have been continental Yangtze craton (Figure 16c,d) or a marginal basin (Figure 16b). The E–W trend of the southern margin of the Sino–Korean craton in the Qinling–Dabie area, coupled with the observed motion within the extrusion channel, implies that the UHP slab was extruded eastward along the plate margin during exhumation (Figure 16e). We suggest that this occurred toward an eastern reentrant in the plate margin that imposed a weak constraint on the extruding lithosphere (Figure 1).

This extrusion geometry requires a complex displacement gradient across the extruding wedge and into its southern and eastern foreland (Figure 16e). The most northerly and most deeply subducted UHP rocks experienced the largest amount of vertical and lateral displacement, which progressively diminished southward and westward toward the lower P units; the plate-margin oblique motion imposed a dextral displacement gradient within the exhuming slab. The vertical shortening, the north dip of the subducting slab, the dextral displacement gradient, and the ongoing shortening due to Yangtze–Sino–Korean plate convergence probably all contributed to the formation of the <a> folds and their northward overturning; the angular divergence between the NW plunge of the stretching lineation and the WNW

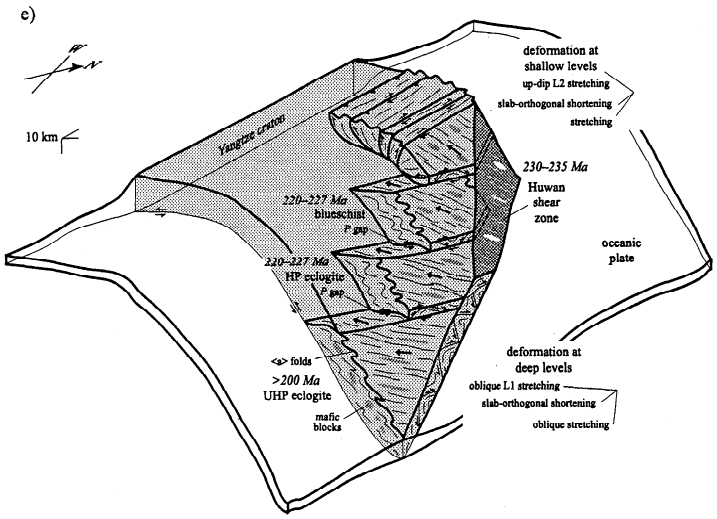

Figure 16. (continued)

plunge of the <a> folds is compatible with the inferred dextral displacement gradient. Lineations in Hong'an–Dabie that swing from an early SE plunge through a late SW plunge mean either that the component of lateral (SE directed) flow diminished with time and became mostly updip, that contraction across the plate margin increased with time, or that the slab rotated clockwise.

Deformation in the Lower Yangtze fold–thrust belt was driven by deformation in the orogen core. SE directed extrusion of the UHP rocks must have induced equivalent shortening at the tip of the extruding wedge. The dominantly SE directed extrusion and the wedge shape of the extruded slab caused shortening in the foreland SE of Dabie and dextral transpression south of Dabie (Figure 4 and *Schmid et al.* [2000]). Moreover, the oroclinal bend in the foreland, from its NE trend east of Dabie to its east trend south of Dabie, is at least partly a reflection of this along-strike change in deformation mode (orthogonal to dextral transpressive shortening).

The footwall beneath the extruding slab might initially have been oceanic (promontory model, Figure 16b) and only later continental crust now comprising the Lower Yangtze fold–thrust belt. The shape of such a (speculative) marginal oceanic basin would have had paramount influence on the exhumation process because an extruding continental slab is always buoyant relative to oceanic lithosphere, whereas a continental crustal slab is only buoyant below the Moho in continental lithosphere. In other words, the slab should have thrust preferentially over oceanic rather than continental footwall. A weakness of our model is that we cannot identify a sole thrust along the southern and eastern edges of Dabie–Hong'an. The southern edge is buried beneath the sediments of the Yangtze river. Along the eastern edge such a fault could be covered by the ubiquitous younger sedimentary rocks, but one of the characteristics of the Triassic/Jurassic foreland deformation east of Dabie is upright folding and a combination of hinterland- and foreland-directed thrusting [*Schmid et al.*, 2000] with relatively moderate shortening. To explain the apparent lack of the megathrust and the distinctive structural style, we postulate that the leading edge of the UHP–HP rocks forms a wedge that is buried beneath the cover strata of the foreland. This implies that the crust of the foreland was detached at middle to upper crustal levels and thrust northwestward onto the crystalline core (Figure 16d; note, however, that this section is at a high angle to the transport direction).

In this scenario the oldest Triassic zircon ages at ~240 Ma (Middle Triassic) reflect recrystallization at peak pressure, and the oldest muscovites in the Huwan shear zone preserve initial exhumation at 230–235 Ma (also Middle Triassic). This interpretation is consonant with the sedimentary record [*Han et al.*, 1989; *Sun et al.*, 1989; *Wang et al.*, 1989; *Zhang et al.*, 1989]. Sedimentary rocks north and south of the suture show shallow marine sedimentation through the Permian. Nonmarine sedimentation ended along the southern margin of the Sino–Korean craton in the Early Triassic. In contrast, although collision-related(?) shortening began in the Early to Middle Triassic in Sichuan and Zhejiang, the change to nonmarine sedimentation on the Yangtze craton was delayed until the Late Triassic, when it affected the entire northern margin of the craton. Throughout the Triassic the Songpan–Ganze flysch accumulated [*Nie et al.*, 1994; *Zhou and Graham*, 1996]. Unconformities in the basins surrounding the orogen document deformation at the Triassic/Jurassic, Early/Middle Jurassic, Middle/Late Jurassic, and Late Jurassic/Early Cretaceous boundaries. This deformation is recorded in the orogen core, as muscovite and zircon ages, only through ~170 Ma, indicating that by the Middle Jurassic the orogen core was cold.

7. Conclusions

The orogen-scale structure of the Dabie–Hong'an area is an antiform. The north limb has north dipping foliation, north plunging lineation, and top-north shear sense formed as the footwall UHP–HP rocks were drawn southeastward out from beneath the low-grade hanging wall. The south limb carries similar structures that have been rotated through horizontal to southward inclinations. Both limbs carry NE-vergent kilometer-scale folds that are oblique to the stretching lineation, which on the south limb rotated from an early SE trend to a late SW trend, revealing clockwise rotation of the slab about a southwestern pivot during exhumation. We propose that these features resulted

from subduction of an asymmetric continental fragment or promontory whose buoyancy with respect to the mantle varied along strike. Cross sections and reconstructions indicate that the continental slab had a downdip extent >150 km, an along-strike extent >150 km, and a thickness >10 km. U/Pb zircon and $^{40}Ar/^{39}Ar$ muscovite and K-feldspar ages imply that the exhumation terminated diachronously in different units, from ~230 to 210 Ma. Widespread younger isotopic ages record deformation and amphibolite-facies retrograde metamorphism at crustal depths as a result of continued convergence between the Sino–Korean and Yangtze cratons.

Acknowledgments. This research was funded by NSF grants EAR-9417958 and EAR-9796119, and DFG grants Ra442/4, Ra442/9, and Ra442/14. Frank Spera kindly allowed use of his IBM 43P computer in the Magma Dynamics Laboratory at UCSB for K-feldspar $^{40}Ar/^{39}Ar$ spectrum modeling. We thank Dave Rowley, the Stanford Asia group, Jens and Robert Schmid, and numerous Chinese colleagues for discussion and field guidance. Gerold Zeilinger and Jürgen Elias contributed U-stage work. Elizabeth Eide, Aral Okay, and Roberta Rudnick provided perceptive reviews.

References

Ames, L., G. Zhou, and B. Xiong, Geochronology and geochemistry of ultrahigh-pressure metamorphism with implications for collision of the Sino–Korean and Yangtze cratons, central China, *Tectonics*, *15*, 472-489, 1996.

Angelier, J., Fault-slip analysis and paleostress reconstruction, in *Continental Deformation*, edited by P.L. Hancock, pp. 53-100, Pergamon, Tarrytown, N.Y., 1994.

Blumenfeld, P., D. Mainprice, and J.-L. Bouchez, C-slip in quartz from subsolidus deformed granite, *Tectonophysics*, *127*, 97-115, 1986.

Bruguier, O., J.R. Lancelot, and J. Malavielle, U–Pb dating on single detrital zircon grains from the Triassic Songpan–Ganze flysch (central China): Provenance and tectonic correlations, *Earth Planet. Sci. Lett.*, *152*, 217–231, 1997.

Cao, R., and S. Zhu, The Dabieshan coesite-bearing eclogite terrain: a neo-Archean ultra-high pressure metamorphic belt, *Acta Geol. Sin.*, *69*, 232–242, 1995.

Carswell, D.A., P.J. O'Brien, R.N. Wilson, and M. Zhai, Thermobarometry of phengite-bearing eclogites in the Dabie Mountains of central China, *J. Metamorph. Geol.*, *15*, 239–252, 1997.

Chavagnac, V., and B.-m. Jahn, Coesite-bearing eclogites from the Bixiling Complex, Dabie Mountains, China; Sm-Nd ages, geochemical characteristics and tectonic implications, *Chem. Geol.*, *133*, 29-51, 1996.

Chemenda, A.I., M. Mattauer, J. Malavieille, and A.N. Bokun, A mechanism for syn-collisional rock exhumation and associated normal faulting: Results from physical modelling, *Earth Planet. Sci. Lett.*, *132*, 225-232, 1995.

Chen, J., Z. Xie, S. Liu, X. Li, and K.A. Foland, Cooling age of Dabie orogen, China, determined by ^{40}Ar-^{39}Ar and fission track techniques, *Sci. China, Ser. B*, *38*, 749–757, 1995.

Cobbold, P., and H. Quinquis, Development of sheath folds in shear regimes, *J. Struct. Geol.*, *2*, 119-126, 1980.

Cui, W., and X. Wang, Eclogites of southern Henan and northern Hubei province, central China, *Isl. Arc*, *4*, 347–361, 1995.

Eide, E.A., Petrology, geochronology, and structure of high-pressure metamorphic rocks in Hubei province, east-central China, and their relationship to continental collision, Ph.D. thesis, Stanford Univ., Stanford, California, 1993.

Eide, E.A., and J.G. Liou, High-pressure blueschists and eclogites in Hong'an: a framework for addressing the evolution of ultrahigh-pressure rocks in central China, in *Paleozoic and Mesozoic tectonic evolution of central Asia: from continental assembly to intracontinental deformation*, edited by M.S. Hendrix and G.A. Davis, *Spec. Pap. Geol. Soc. Am.*, in press, 2000.

Eide, L., M.O. McWilliams, and J.G. Liou, $^{40}Ar/^{39}Ar$ geochronologic constraints on the exhumation of HP-UHP metamorphic rocks in east-central China, *Geology*, *22*, 601–604, 1994.

Ellis, D.J., and D.H. Green, An experimental study of the effect of Ca upon garnet-clinopyroxene Fe-Mg exchange equilibria, *Contrib. Mineral. Petrol.*, *71*, 13-22, 1979.

Ernst, W.G., and S.M. Peacock, A thermotectonic model for preservation of ultrahigh-pressure phases in metamorphosed continental crust, in *Subduction Top to Bottom*, *Geophys. Monogr. Ser.*, vol. 96, edited by G.E. Bebout et al., pp. 171-178, AGU, Washington, D. C., 1996.

Ernst, W.G., G. Zhou, J.G. Liou, E. Eide, and X. Wang, High-pressure and superhigh-pressure metamorphic terranes in the Qinling-Dabie mountain belt, central China; early to mid-Phanerozoic accretion of the western paleo-Pacific Rim, *Pac. Sci. Assoc. Inf. Bull.*, *43*, 6–15, 1991.

Froitzheim, N., Formation of recumbent folds during synorogenic crustal extension (Austroalpine nappes, Switzerland), *Geology*, *20*, 923-926, 1992.

Gilder, S.A., P.H. Leloup, V. Courtillot, Y. Chen, R. Coe, X. Zhao, W. Xiao, N. Halim, J.-P. Cogne, and R. Zhu, Tectonic evolution of the Tancheng–Lujiang (Tan–Lu) fault via Middle Triassic to Early Cenozoic paleomagnetic data, *J. Geophys. Res.*, *104*, 15,365–15,390, 1999.

Grove, M., Thermal histories of Southern California basement terranes, Ph.D. thesis, Univ. of Calif., Los Angeles, 1993.

Grove, M., and G.E. Bebout, Cretaceous tectonic evolution of coastal southern California: insights from the Catalina schist, *Tectonics*, *14*, 1290–1308, 1995.

Guidotti, C.V., and F.P. Sassi, Petrogenetic significance of Na-K white mica mineralogy: Recent advances for metamorphic rocks, *Eur. J. Mineral.*, *10*, 815-854, 1998.

Hacker, B.R., and S.M. Peacock, Creation, preservation, and exhumation of coesite-bearing, ultrahigh-pressure metamorphic rocks, in *Ultrahigh Pressure Metamorphism*, edited by R.G. Coleman and X. Wang, pp. 159–181, Cambridge Univ. Press, New York, 1995.

Hacker, B.R., and Q.C. Wang, Ar/Ar geochronology of ultrahigh-pressure metamorphism in central China, *Tectonics*, *14*, 994–1006, 1995.

Hacker, B.R., L. Ratschbacher, L. Webb, and S. Dong, What brought them up? Exhumation of the Dabie Shan ultrahigh-pressure rocks, *Geology*, *23*, 743-746, 1995.

Hacker, B.R., J.L. Mosenfelder, and E. Gnos, Rapid ophiolite emplacement constrained by geochronology and thermal considerations, *Tectonics*, *15*, 1230–1247, 1996.

Hacker, B.R., T. Sharp, R.Y. Zhang, J.G. Liou, and R.L. Hervig, Determining the origin of ultrahigh-pressure lherzolites, *Science*, *258*, 702–704, 1997.

Hacker, B.R., L. Ratschbacher, L. Webb, T. Ireland, D. Walker, and S. Dong, U/Pb zircon ages constrain the architecture of the ultrahigh-pressure Qinling–Dabie Orogen, China, *Earth Planet. Sci. Lett.*, *161*, 215–230, 1998.

Hames, W.E., and J.T. Cheney, On the loss of $^{40}Ar^*$ from muscovite during polymetamorphism, *Geochim. Cosmochim. Acta*, *61*, 3863–3872, 1997.

Han, J., S. Zhu, and S. Xu, The generation and evolution of the Hehuai basin, in *Sedimentary Basins of the World*, edited by X. Zhu, pp. 125-135, Elsevier Sci., New York, 1989.

Holland, T.J.B., and R. Powell, An internally consistent thermodynamic data set for phases of petrological interest, *J. Metamorph. Geol.*, *16*, 309-343, 1998.

Kirschner, D.L., M.A. Cosca, H. Masson, and J.C. Hunziker, Staircase $^{40}Ar/^{39}Ar$ spectra of fine-grained white mica: timing and duration of deformation and empirical constraints on argon diffusion, *Geology*, *24*, 747–750, 1996.

Li, S., et al., Collision of the North China and Yangtze blocks and formation of coesite-bearing eclogites: Timing and processes, *Chem. Geol.*, *109*, 89–111, 1993.

Linker, M.F., S.H. Kirby, A. Ord, and J.M. Christie, Effects of compression direction on plasticity and rheology of hydrolytically weakened synthetic quartz at atmospheric pressure, *J. Geophys. Res.*, *89*, 4241-4255, 1984.

Liou, J.G., and R.Y. Zhang, Petrogenesis of an ultrahigh-pressure garnet-bearing ultramafic body from Maowu, Dabie Mountains, east-central China, *Isl. Arc*, *7*, 115–134, 1998.

Liou, J.G., R.Y. Zhang, E.A. Eide, S. Maruyama, X. Wang, and W.G. Ernst, Metamorphism and tectonics of high-P and ultrahigh-P belts in Dabie-Sulu Regions, eastern central China, in *The Tectonic Evolution of Asia*, edited by A. Yin and T.M. Harrison, pp. 300-343, Cambridge Univ., New York, 1996.

Liu, J., and J.G. Liou, Kyanite anthophyllite schist and the southwest extension of the Dabie Mountains ultrahigh to high pressure belt, *Isl. Arc*, *4*, 334–346, 1995.

Liu, J., Z. You, and Z. Zhong, Eclogites from the middle and north of Dabie Mountains in southern Henan and northern Hubei, China, *Sci. China, Ser. D*, *39*, 293–299, 1996.

Lovera, O.M., Computer program to model $^{40}Ar/^{39}Ar$ diffusion data from multidomain samples, *Comput. Geosci.*, *18*, 789–813, 1992.

Lovera, O.M., M. Grove, T.M. Harrison, and K.I. Mahon, Systematic analysis of K-feldspar $^{40}Ar/^{39}Ar$ step heating results; I, Significance of activation energy determinations, *Geochim. Cosmochim. Acta*, *61*, 3171-3192, 1997.

Mainprice, D., J.-L. Bouchez, P. Blumenfeld, and J.M. Tubia, Dominant c slip in naturally deformed quartz: Implications for dramatic plastic softening at high temperature, *Geology*, *14*, 819-822, 1986.

Malavieille, J., Extensional shearing deformation and kilometer-scale "a"-type folds in a Cordilleran metamorphic core complex (Raft River Mountains, Northwestern Utah), *Tectonics*, *6*, 423-448, 1987.

Maruyama, S., H. Tabata, A.P. Nutman, T. Morikawa, and J.G. Liou, SHRIMP U-Pb geochronology of ultrahigh-pressure metamorphic rocks of the Dabie Mountains, central China, *Cont. Dyn.*, *3*, 72–85, 1998.

Mattauer, M., Sur le mecanisme de formation de la schistosite dans l'Himalaya, *Earth Planet. Sci. Lett.*, *28*, 144-154, 1975.

Mattauer, M., P. Matte, H. Maluski, Z. Xu, Q.W. Zhang, and Y.M. Wang, La limite Chine du Nord-Chine du Sud au Paléozoïque et au Trias. Nouvelles données structurales et radiométriques dans le massif de Dabie-Shan (chaîne des Qinling) (Paleozoic and Triassic plate boundary between North and South China; New structural and radiometric data on the Dabie-Shan, eastern China), *C. R. Acad. Sci., Ser. II*, *312*, 1227-1233, 1991.

Means, W.D., Stretching faults, *Geology*, *17*, 893-896, 1989.

Ministry of Geology and Mineral Resources, Geological map of China, Beijing, China, 1991.

Muir, R.J., T.R. Ireland, S.D. Weaver, and J.D. Bradshaw, Ion microprobe dating of Paleozoic granitoids: Devonian magmatism in New Zealand and correlations with Australia and Antarctica, *Chem. Geol.*, *127*, 191-210, 1996.

Nie, S., A. Yin, D.B. Rowley, and Y. Jin, Exhumation of the Dabie Shan ultrahigh-pressure rocks and accumulation of the Songpan–Ganzi flysch sequence, central China, *Geology*, *22*, 999–1002, 1994.

Okay, A.I., Petrology of a diamond and coesite-bearing metamorphic terrain: Dabie Shan, China, *Eur. J. Mineral.*, *5*, 659–675, 1993.

Okay, A.I., Sapphirine and Ti-clinohumite in ultra-high-pressure garnet-pyroxenite and eclogite from Dabie Shan, China, *Contrib. Mineral. Petrol.*, *116*, 145-155, 1994.

Okay, A.I., A.M.C. Sengör, and M. Satir, Tectonics of an ultrahigh-pressure metamorphic terrane: the Dabie Shan/Tongbai Shan orogen, China, *Tectonics*, *12*, 1320–1334, 1993.

Passchier, C.W., and R.A.J. Trouw, *Microtectonics*, 289 pp., Springer–Verlag, New York, 1996.

Platt, J.P., Secondary cleavages in ductile shear zones, *J. Struct. Geol.*, *6*, 439-442, 1984.

Platt, J.P., and R.L.M. Vissers, Extensional structures in anisotropic rocks, *J. Struct. Geol.*, *2*, 397-410, 1980.

Ratschbacher, L., and G. Oertel, Superposed deformation in the eastern Alps: strain analysis and microfabrics, *J. Struct. Geol.*, *9*, 263-276, 1987.

Ravna, E.K., The garnet-clinopyroxene geothermometer - an updated calibration, *Eos. Trans. AGU*, *79*(45), Fall Meet. Suppl., F999, 1998.

Ree, J.-H., M. Cho, S.-T. Kwon, and E. Nakamura, Possible eastward extension of Chinese collision belt in South Korea; the Imjingang Belt, *Geology*, *24*, 1071-1074, 1996.

Regional Geological Survey of Anhui, Regional geology of Anhui Province, scale 1:500,000, Geol. Publ. House, Beijing, 1987.

Regional Geological Survey of Henan, Regional geology of Henan Province, scale 1:500,000, Geol. Publ. House, Beijing, 1989.

Regional Geological Survey of Hubei, Regional geology of Hubei Province, scale 1:500,000, Geol. Publ. House, Beijing, 1990.

Ratschbacher, L., B.R. Hacker, L.E. Webb, M.O. McWilliams, T.R. Ireland, S. Dong, A. Calvert, D. Chateigner, and H.-R. Wenk, Exhumation of ultrahigh-pressure continental crust in east central China: Cretaceous and Cenozoic unroofing and the Tan-Lu fault, *J. Geophys. Res.*, this issue.

Roddick, J.C., The application of isochron diagrams in ^{40}Ar-^{39}Ar dating: a discussion, *Earth Planet. Sci. Lett.*, *41*, 233–244, 1978.

Rowley, D.B., and F. Xue, Modeling the exhumation of ultra-high pressure metamorphic assemblages; observations from the Dabie/Tongbai region, China, *Geol. Soc. Am. Abstr. Programs*, *28*, 249, 1996.

Rowley, D.B., F. Xue, R.D. Tucker, Z.X. Peng, J. Baker, and A. Davis, Ages of ultrahigh pressure metamorphism and protolith orthogneisses from the eastern Dabie Shan: U/Pb zircon geochronology, *Earth Planet. Sci. Lett.*, *151*, 191–203, 1997.

Sanderson, D., The development of fold axes oblique to the regional trend, *Tectonophysics*, *16*, 55-70, 1973.

Scaillet, S., K–Ar ($^{40}Ar/^{39}Ar$) geochronology of ultrahigh pressure rocks, in *When Continents Collide: Geodynamics and Geochemistry of Ultrahigh-Pressure Rocks*, edited by B.R. Hacker and J.G. Liou, pp. 161–201, Kluwer Acad., Norwell, Mass., 1998.

Schmid, S.M., and M. Casey, Complete fabric analysis of some commonly observed quartz c-axis patterns, in *Mineral and Rock Deformation: Laboratory Studies, The Paterson Volume, Geophys. Mon. Ser.*, vol. 36, pp. 263–286, 1986.

Schmid, J.C., L. Ratschbacher, I. Gaitzsch, B.R. Hacker, and S. Dong, Triassic to Recent Dabie Shan foreland deformation, *Terra Nova*, in press, 2000.

Spang, J.H., Numerical method for dynamic analysis of calcite twin lamellae, *Geol. Soc. Am. Bull.*, *83*, 467-471, 1972.

Sun, Z., Q. Xie, and J. Yang, Ordos Basin: a typical example of an unstable cratonic interior superimposed basin, in *Sedimentary Basins of the World*, edited by X. Zhu, pp. 63-75, Elsevier Sci., New York, 1989.

Tsai, C.-H., and J.G. Liou, Eclogite facies relics and inferred ultrahigh-pressure metamorphism in the North Dabie Complex, central-eastern China, *Am. Mineral.*, *85*, 1–8, 2000.

Turner, F.J., Nature and dynamic interpretation of deformation lamellae in calcite of three marbles, *Am. J. Sci.*, *251*, 276–298, 1953.

Twiss, R.J., and J.R. Unruh, Analysis of fault slip inversions: Do they constrain stress or strain rate?, *J. Geophys. Res.*, *103*, 12205–12221, 1998.

Wang, Q., C. Bao, Z. Lou, and Z. Guo, Formation and development of the Sichuan basin, in *Sedimentary Basins of the World*, edited by X. Zhu, pp. 147-163, Elsevier Sci., New York, 1989.

Watkinson, A.J., Multilayer folds initiated in bulk plane strain with the axis of no change perpendicular to layering, *Tectonophysics*, *28*, 7-11, 1975.

Webb, L.E., B.R. Hacker, L. Ratschbacher, and S. Dong, Thermochronologic constraints on deformation and cooling history of high and ultrahigh-pressure rocks in the Qinling-Dabie orogen, eastern China, *Tectonics*, *18*, 621–637, 1999.

Webb, L.E., B.R. Ratschbacher, Hacker, L. and S. Dong, Kinematics of exhumation of high- and ultrahigh-pressure rocks in the Hong'an and Tongbai Shan of the Qinling–Dabie collisional orogen, eastern China, in *Paleozoic and Mesozoic Tectonic Evolution of Central Asia: from Continental Assembly to Intracontinental Deformation*, edited by M.S. Hendrix and G.A. Davis, *Spec. Pap. Geol. Soc. Am.*, in press, 2000.

Wendt, I., and C. Carl, The statistical distribution of the mean squared weighted deviation, *Chem. Geol.*, *86*, 275–285, 1991.

Xu, S., and W. Su, Raman determination on micro-diamond in eclogite from the Dabie Mountains, eastern China, *Chin. Sci. Bull.*, *42*, 87, 1997.

Xue, F., A. Kröner, T. Reischmann, and F. Lerch, Palaeozoic pre- and post-collision calc-alkaline magmatism in the Qinling orogenic belt, central China, as documented by zircon ages on granitoid rocks, *J. Geol. Soc. London*, *153*, 409–417, 1996.

Xue, F., D.B. Rowley, R.D. Tucker, and Z.X. Peng, U-Pb zircon ages of granitoid rocks in the north Dabie complex, eastern Dabie Shan, China, *J. Geol.*, *105*, 744–753, 1997.

Yin, A., and S. Nie, An indentation model for the North and South China collision and the development of the Tanlu and Honam fault systems, eastern Asia, *Tectonics*, *12*, 801–813, 1993.

Zhai, X., H.W. Day, B.R. Hacker, and Z. You, Paleozoic metamorphism in the Qinling orogen, Tongbai Mountains, central China, *Geology*, *26*, 371–374, 1998.

Zhang, Y., Z. Wei, W. Xu, R. Tao, and R. Chen, The North Jiangsu–South Yellow Sea basin, in *Sedimentary Basins of the World*, edited by X. Zhu, pp. 107-123, Elsevier Sci., New York, 1989.

Zhao, X., and R.S. Coe, Palaeomagnetic constraints on the collision and rotation of North and South China, *Nature*, *327*, 141-144, 1987.

Zhou, D., and S.A. Graham, Songpan-Ganzi complex of the west Qinling Shan as a Triassic remnant ocean basin, in *The Tectonic Evolution of Asia*, edited by A. Yin and T.M. Harrison, pp. 281-299, Cambridge Univ., New York, 1996.

Zhou, G., J. Liu, E.A. Eide, J.G. Liou, and W.G. Ernst, High-pressure/low-temperature metamorphism in northern Hubei Province, central China, *J. Metamorph. Geol.*, *11*, 561–574, 1993.

A. Calvert and B. R. Hacker, Department of Geology, University of California, Santa Barbara, CA, 93106-9630. (calvert@geology.ucsb.edu; hacker@geology.ucsb.edu)

D. Chateigner, Laboratoire de Physique de l'Etat Condensé, Universite du Maine, av. O. Messiaen, BP535 F-72085, Le Mans Cedex 9, France.

S. Dong, Chinese Academy of Geological Sciences, No. II, Ming zhu Xueyang Road, 100081, Beijing, People's Republic of China. (swdong@public.fhnet.cn.net)

T. Ireland, and M. O. McWilliams, Department of Geological and Environmental Sciences, Stanford University, Stanford, CA 94305-2115. (tri@geo.stanford.edu; mac@geo.stanford.edu)

L. Ratschbacher, Institut für Geologie, Technische Universität Bergakademie Freiberg, Bernhard-von-Cotta-Str. 2, D-09596 Freiberg/Sachsen, Germany. (lothar@geo.tu-freiberg.de)

L. Webb, Section des Sciences de la Terre, Université de Geneve, 13 rue des Maraichers, CH-1211 Geneva 4, Switzerland. (laura.webb@terre.unige.ch)

H.-R. Wenk, Department of Geology, University of California, Berkeley, CA 94720-4767. (wenk@seismo.berkeley.edu)

(Received June 28, 1999; revised December 31, 1999;
accepted January 25, 2000.)